Available online at www.sciencedirect.com

ScienceDirect

Geochimica et Cosmochimica Acta 148 (2015) 343–359

Geochimica et Cosmochimica Acta

www.elsevier.com/locate/gca

U(VI) behaviour in hyperalkaline calcite systems

Kurt F. Smith [a,b], Nicholas D. Bryan [b,c], Adam N. Swinburne [c], Pieter Bots [a], Samuel Shaw [a], Louise S. Natrajan [c], J. Frederick W. Mosselmans [d], Francis R. Livens [a,c], Katherine Morris [a,*]

[a] *Research Centre for Radwaste Disposal and Williamson Research Centre, School of Earth, Atmospheric and Environmental Sciences, The University of Manchester, Oxford Road, Manchester M13 9PL, United Kingdom*

[b] *National Nuclear Laboratory, Chadwick House, Risley WA3 6AE, United Kingdom*

[c] *Centre for Radiochemistry Research, School of Chemistry, The University of Manchester, Oxford Road, Manchester M13 9PL, United Kingdom*

[d] *Diamond Light Source Ltd., Diamond House, Harwell Science and Innovation Campus, Didcot, Oxfordshire OX11 0DE, United Kingdom*

Received 20 March 2014; accepted in revised form 30 September 2014; available online 13 October 2014

Abstract

The behaviour of U(VI) in hyperalkaline fluid/calcite systems was studied over a range of U(VI) concentrations (5.27×10^{-5} μM to 42.0 μM) and in two high pH systems, young and old synthetic cement leachate in batch sorption experiments. These systems were selected to be representative of young- (pH 13.3) and old-stage (pH 10.5) leachate evolution within a cementitious geological disposal facility. Batch sorption experiments, modelling, extended X-ray absorption fine structure spectroscopy, electron microscopy, small angle X-ray scattering and luminescence spectroscopy were used to define the speciation of U(VI) across the systems of study. At the lowest concentrations (5.27×10^{-5} μM ^{232}U(VI)) significant U removal was observed for both old and young cement leachates, and this was successfully modelled using a first order kinetic adsorption modelling approach. At higher concentrations (>4.20 μM) in the young cement leachate, U(VI) showed no interaction with the calcite surface over an 18 month period. Small angle X-ray scattering techniques indicated that at high U concentrations (42.0 μM) and after 18 months, the U(VI) was present in a colloidal form which had little interaction with the calcite surface and consisted of both primary and aggregated particles with a radius of 7.6 ± 1.1 and 217 ± 24 Å, respectively. In the old cement leachate, luminescence spectroscopy identified two surface binding sites for U(VI) on calcite: in the system with 0.21 μM U(VI), a liebigite-like $Ca_2UO_2(CO_3)_3$ surface complex was identified; at higher U(VI) concentrations (0.42 μM), a second binding site of undetermined coordination was identified. At elevated U(VI) concentrations (>2.10 μM) in old cement leachate, both geochemical data and luminescence spectroscopy suggested that surface mediated precipitation was controlling U(VI) behaviour. A focused ion beam mill was used to create a section across the U(VI) precipitate–calcite interface. Transmission electron microscope images of the section revealed that the calcite surface was coated with a nano crystalline, U containing phase. Selected area electron diffraction images of the U precipitate which was formed at a U(VI) concentration of 4.20 μM were consistent with the formation of calcium uranate. XAS spectroscopy at higher concentrations (⩾21.0 μM) suggested the formation of a second U(VI) phase, possibly a uranyl oxyhydroxide phase.

These results indicated that in the young cement leachate, U(VI) did not react with the calcite surface unless U(VI) concentrations were very low (5.27×10^{-5} μM). At higher concentrations, speciation calculations suggested that U(VI) was significantly oversaturated and experimental observations confirmed it existed in a colloidal form that interacted with the mineral surface only weakly. In the old cement leachate systems at low concentrations batch sorption and luminescence data suggested that U(VI) removal was being driven by a surface complexation mechanism. However, at higher concentrations, spectroscopic methods suggest a combination of both surface complexation and surface mediated precipitation was

* Corresponding author.
E-mail address: katherine.morris@manchester.ac.uk (K. Morris).

http://dx.doi.org/10.1016/j.gca.2014.09.043

responsible for the observed removal. Overall, U(VI) behaviour in hyperalkaline calcite systems is distinct from that at circumneutral pH conditions: at high pH and anything but low U(VI) concentrations, a surface mediated precipitation mechanism occurs; this is in contrast to circumneutral pH conditions where U(VI) surface complexation reactions tend to dominate.

1. INTRODUCTION

In many countries the long-term management of intermediate level radioactive wastes will be for their final disposal in a deep Geological Disposal Facility (GDF) (NEA, 2004; DEFRA, 2008; Schwyn et al., 2012). The GDF will be designed to isolate radionuclides from the biosphere for sufficient time to allow the majority of the radioactive material to undergo radioactive decay, although for longer lived radionuclides it is clear that transport away from the engineered barrier cannot be ruled out. Once the waste has been packaged, typically by grouting in steel drums, it will be emplaced in the facility and backfilled. Currently it is anticipated that in the UK, the GDF will be backfilled with cementitious material, and engineering cement (e.g. "shotcrete") will be utilised in many designs. This means that consideration of the alkaline conditions that result from cement materials is of wide relevance (Schmidt, 1991; Schwyn et al., 2012). The cementitious environment is expected to remain alkaline (i.e. pH 10.5–13.1) over extended periods and, in the saturated sub-surface, is intended to produce conditions that reduce radionuclide mobility due to formation of insoluble hydrolysis products and increased sorption of cations to negatively charged mineral surfaces (Braney et al., 1993). In a cementitious GDF over time, the portlandite ($Ca(OH)_2$) and calcium silicate hydrate (C–S–H) components of the cement will undergo carbonation via reaction with carbonate in groundwaters to form minerals including calcite ($CaCO_3$; Dow and Glasser, 2003). This will increase the quantity of calcite present in any evolved cementitious GDF. Calcite is also ubiquitous in the natural environment and may well be a component of the host rock environment. Calcite has been shown to sequester metals and radionuclides effectively by adsorption and/or incorporation (Zachara et al., 1991; Geipel et al., 1997; Parkman et al., 1998; Hay et al., 2003; Rihs et al., 2004; Dong et al., 2005; Zavarin et al., 2005; Heberling et al., 2008). Thus, calcite clearly has the potential to be an important reactive mineral phase for radionuclides within the GDF environment.

U(VI) is stable in oxidising environments, readily forms the linear uranyl moiety ($O = U = O$; UO_2^{2+}) and typically has increased mobility compared to U(IV). In addition, under the hyperalkaline to alkaline conditions relevant to this study, U(VI) is expected to remain stable under anoxic and modestly reducing conditions (Gaona et al., 2011). Certain studies concerning U(VI) interactions with calcite have focused on incorporation and coprecipitation (Meece and Benninger, 1993; Curti, 1999; Reeder et al., 2000, 2001; Kelly et al., 2003; Elzinga et al., 2004), whilst others have studied sorption (Carroll et al., 1992; Geipel et al., 1997; Elzinga et al., 2004; Rihs et al., 2004). In an evolving geological disposal facility, the geochemical environment will be dynamic and both sorption and incorporation/coprecipitation reactions with radionuclides are possible.

There is a significant literature on U(VI) calcite interactions at ambient pH, for example, Elzinga et al. (2004) studied the reaction of U(VI) with calcite at pH 7.4 and 8.3 and over the concentration range 5 to 5000 μM using batch sorption experiments, Extended X-ray Absorption Fine Structure (EXAFS) and luminescence spectroscopy. EXAFS analysis of their batch sorption experiments with <500 μM U(VI) produced data consistent with the formation of uranyl triscarbonate surface complexes and suggested that sorption in their systems was taking place via inner sphere complexation, in agreement with Rihs et al. (2004). Unfortunately, their EXAFS analysis could not identify any calcium backscatterers to corroborate the proposed inner sphere bonding, and thus the exact coordination environment of U(VI) in this system remained undetermined. The authors then used luminescence spectroscopy to explore whether different U(VI) surface species were present in their experiments: at <100 μM U(VI) a calcium uranyl triscarbonate complex (in a liebigite-like structure) dominated, whilst for systems in the 100–500 μM range, there was evidence that a different, undetermined uranyl carbonate species became significant. The authors suggested this undetermined phase was likely to be intermediate between the liebigite-like ($Ca_2UO_2(CO_3)_3$) surface complex and U(VI) incorporated into calcite. Indeed, EXAFS and luminescence techniques confirm that when UO_2^{2+} is coprecipitated with calcite, it can exist in multiple coordination environments dependent on the method of precipitation (Reeder et al., 2000, 2001). Furthermore, it has been shown that selective incorporation of UO_2^{2+} during calcite coprecipitation takes place on the '-' steps of the calcite (1 0 4) surface (Reeder et al., 2004; Rihs et al., 2004). Refinement of this concept by Rihs et al. (2004) suggested that the number of binding sites in their experimental system was too low to account for the U(VI) sorption they observed, and that additional sites could be provided by calcium vacancies or "etch pits", which are effectively equivalent to additional '-' steps. Recent computational molecular dynamics simulations (Doudou et al., 2012) support preferential sorption of the $Ca_2UO_2(CO_3)_{3(aq)}$ species onto the '-' steps but also suggest that outer sphere complexation on the calcite terrace should be thermodynamically favourable. In addition to surface complexation and incorporation, calcite has been shown to promote the formation of U(VI) precipitates, such as schoepite ($(UO_2)_8O_2(OH)_{12}\cdot 12H_2O$; Carroll et al., 1992; Geipel et al., 1997; Elzinga et al., 2004; Schindler and Putnis, 2004).

Overall, these studies have developed a good understanding of U(VI) behaviour in calcite systems, including incorporation and surface complexation mechanisms. However, most studies have focused on ambient environmental conditions, whilst in any cementitious GDF, alkaline pH conditions will prevail with pH values >10.5 dominating over 10^5–10^6 years and with elevated ionic strength compared to typical environmental conditions. This gap in knowledge needs to be addressed in order to underpin any performance assessment for a cementitious GDF. Here, we examine U(VI) interactions with calcite under the hyperalkaline conditions representative of an early stage evolution "young" and late stage evolution "old" GDF using synthetic Young Cement Leachate (YCL) and Old Cement Leachate (OCL). We present data from batch sorption experiments using varying solid to solution ratios and a wide range of U(VI) concentrations, to develop a mechanistic understanding of U(VI) behaviour across relevant alkaline calcite systems. Batch sorption experiments, geochemical modelling, EXAFS, electron microscopy, Small Angle X-ray Scattering (SAXS) and luminescence spectroscopy have been applied to probe the fate and speciation of U(VI) in these experiments.

2. METHODOLOGY

2.1. Modelling

All thermodynamic modelling was carried out with PHREEQC 3.0.0 using the ANDRA SIT database (ThermoChimie v.7.d June 2011). The database was modified to include the formation constant for $Ca_2UO_2(CO_3)_{3(aq)}$ (Bernhard et al., 2001).

All kinetic modelling was carried out in R (R-Core, 2012). The data were modelled with a simple, first order kinetic adsorption model that assumed the sorption site concentration was proportional to the mass of calcite. The chemical equation used in the kinetic modelling was,

$$M + S \underset{k_2}{\overset{k_1}{\leftrightarrow}} M_S \quad (1)$$

and the rate equation was,

$$\frac{d[M]}{dt} = k_1[M][S] - k_2[M_S] \quad (2)$$

where [M] refers to the metal concentration, [S] is the concentration of calcite surface binding sites, $[M_S]$ is the concentration of U(VI) associated with surface binding sites and k_1 and k_2 are the forward and backward rate constants, respectively. The calcite binding site density value was arbitrary as in experiments, saturation of surface binding sites was not approached. However, the use of this arbitrary value did not affect the goodness of fit, as the calcite binding site concentration acts as a scaling constant: for example, if the true value of [S] were lower, then k_1 would increase proportionately, but the fit would not change. In other words, the experimental data provided us with only the product, $k_1[S]$, not the absolute, separate values of the rate constant and surface site concentration. A value of 1 for surface binding site concentration [S] was used for modelling experimental data with a 0.1 kg L^{-1} solid to solution ratio and then adjusted proportionately for different solid to solution ratios.

2.2. Sorption experiments

U(VI) behaviour was studied in batch sorption experiments where the systems were pre-equilibrated with calcite prior to U(VI) additions. All chemicals used were analytical reagent grade and all solutions were made using Milli-Q (18.2 M Ω cm) water. In addition, all experiments and sample manipulations were performed in a CO_2 free environment. The calcite used in this study was a purchased high purity crystalline powder prepared by precipitation (SureChem Products Ltd) and was characterised via powder X-ray diffraction (see supporting information; Figure S1; Bruker D8 Advance). Prior to use, the calcite was passed through a <63 μm sieve, and the surface area of this sieved material was measured as 0.26 ± 0.01 m^2 g^{-1} using N_2 B.E.T analysis. Depleted uranium as $UO_2(NO_3)_2$ (BDH), was dissolved in 0.01 M HCl to give a stock solution concentration of 0.02 M. Uranium tracer (^{232}U(VI) in 2 M HNO_3; AREVA) was separated from ingrown ^{228}Th using ion exchange to allow Liquid Scintillation Counting (LSC) of ^{232}U, without interference from ^{228}Th and its daughters (Ong and Leckie, 1996).

For experiments at ultra-trace U(VI) concentrations, the experiments were spiked with ^{232}U to a concentration of 5.27×10^{-5} μM (10 Bq mL^{-1}). For analysis, a 1 mL sample was mixed with scintillant (Scintisafe 3, Fisher Scientific) and 2 mL 1 M HCl, prior to counting on a LSC (Quantulus, PerkinElmer) instrument with appropriate, matrix matched standards. In this conformation, the detection limit was ~0.1 Bq mL^{-1} and the count time was adjusted such that the counting error was 5% or less. In experiments bracketing the higher U(VI) concentration range (0.21–42.0 μM), U(VI) was used and concentrations were determined using ICP-MS (Agilent 7500cx), again with appropriate, matrix matched standards. All experiments were run in triplicate.

This work used two different synthetic solutions that reflected the chemical conditions (particularly pH and calcium concentrations) expected during the evolution of cement in contact with flowing water: OCL; and YCL (Table 1), either as made, or equilibrated for four days with calcite and then filtered (<0.45 μm; Whatman nylon filter). During preparation to avoid oversaturation, the YCL solution was kept in a CO_2 free environment in an oven at 40 °C for 48 h prior to filtration through a 0.45 μm nylon filter. Selected calcite pre-equilibrated experiments using YCL,

Table 1
Synthetic cement leachate solution composition.

	OCL	YCL
pH	10.5	13.3
KOH (g L^{-1})	–	5.2
NaOH (g L^{-1})	–	3.8
$Ca(OH)_2$ (g L^{-1})	0.015	0.01

OCL and Milli-Q water were also run, which were equilibrated with calcite for four days, prior to filtration through a 0.45 μm nylon filter.

Batch sorption experiments with solid to solution ratios between 1:500 and 1:2 were carried out. In these experiments, the calcite was mixed with the OCL or YCL and allowed to equilibrate with the solution for four days prior to spiking with ^{232}U or U solutions. For higher U(VI) concentrations, the solutions were spiked from a 2.5 mM U(VI) stock solution in 0.01 M HCl to yield final U concentrations between 0.21 and 42 μM. For ultra-trace experiments, ^{232}U in 0.01 M HCl was added to give a final concentration of (5.27×10^{-5} μM/10 Bq mL^{-1}). All experiments were performed in triplicate unless otherwise stated.

2.3. Luminescence spectroscopy

In order to assess U(VI) speciation across the lower range of experimental concentrations, luminescence spectroscopy was used. Once batch data suggested that the experiments had reached equilibrium, U(VI) labelled calcite samples (2.5–1000 ppm on solids) were prepared for luminescence spectroscopy by centrifugation (500 g, 5 min) to leave a moist paste which was then mounted in a Suprasil quartz tube.

Steady state emission spectra were recorded at 77 K using an Edinburgh Instrument FP920 Phosphorescence Lifetime Spectrometer equipped with a 5 W microsecond pulsed xenon flashlamp (with single 300 mm focal length excitation and emission monochromators in Czerny Turner configuration) and a red sensitive photomultiplier in a Peltier housing (air cooled, Hamamatsu R928P). Where indicated, delay time and gate time were applied during emission measurements. Lifetime data were recorded following excitation with a microsecond xenon flashlamp, using the multi-channel scaling method. Lifetimes were obtained by tail fit on the data, and the quality of fit judged by minimization of reduced χ^2 and residuals squared. Where the decay profiles are reported as mono-exponential, fitting to a double exponential gave no significant improvement in fit.

2.4. Electron microscopy

U(VI)–calcite precipitates were examined using both Scanning- and Transmission–Electron Microscopy (SEM/TEM). The SEM images were collected on a FEI Nova200 dual beam SEM/Focused Ion Beam (FIB) in backscatter electron imaging. SEM samples were mounted on a carbon pad, carbon coated and imaged. A thin section (approximately 10 μm × 8 μm × 150 nm) was prepared using a FIB fitted utilising Kleindiek micromanipulators. The thin section was then analysed with TEM using a FEI Tecnai F20 FEGTEM instrument, fitted with a Gatan Orius SC600 CCD camera. The thin section was imaged in high magnification mode and in High-Angle Annular Dark-Field (HAADF) mode to obtain Z contrast images. In addition, Selected Area Electron Diffraction (SAED) patterns were collected. Energy Dispersive X-ray (EDX) analysis was carried out on a Philips CM200 FEG-TEM fitted with an Oxford Instruments 80 mm^2 X-Max SDD detector.

2.5. Extended X-ray absorption fine structure spectroscopy

Selected U(VI) reacted calcite samples (500 – 1000 ppm) were prepared for EXAFS spectroscopy by centrifuging (500 g, 5 min) before separating the moist paste for analysis. The solid sample (~0.2 g) was then mounted in a CO_2 free environment onto a Perspex sample holder and sealed with Kapton tape. The sample holder was then heat sealed in a CO_2 free argon environment and the sample stored at 4 °C prior to analysis. EXAFS spectra were collected for the U L_{III}-edge on B18 at the Diamond Light Source using a 9 element solid-state Ge detector, focusing optics (beam size 0.5 mm^2), and a Si-111 double crystal monochromator. Data collection was carried out at room temperature. Between 8 and 20 QEXAFS scans were collected per sample and averaged in order to increase the signal to noise ratio. Scans were normalised in energy space using an inline yttrium metal reference standard. Background processing was performed using Athena, and EXAFS modelling was carried out using Artemis (Demeter; 0.9.14; Ravel and Newville, 2005). All fitting was carried out using k^1, k^2, and k^3 (typical range, 3–12 k), while the best fit was calculated in R space (typical range, 1–4.2 Å) by minimisation of the fit index, R. The reduced χ^2 term was used to assess the significance of extra shells in the fit. A forward through absorber Multiple Scattering (MS) path was included for the axial 'yl' oxygen atoms, where it offered an improvement in the fit (Catalano and Brown, 2004). In the fitting of the U–O_{axial} MS path, the parameters for distance and the Debye–Waller-like factor (σ^2) were set to double the values for the U–O_{axial} single scattering path (Catalano and Brown, 2004). In all cases, the inclusion of the U–O_{axial} MS path did not require any additional parameters, and in all cases parameterisation used no more than two thirds of the total number of available independent data points.

2.6. Small angle X-ray scattering

Small angle X-ray scattering was used to investigate the U(VI) colloidal particles in calcite equilibrated YCL solutions. The SAXS samples were prepared by spiking a calcite pre-equilibrated YCL solution to 42.0 μM U(VI) with a 2.5 mM U(VI) stock solution (in 0.01 M HCl). The sample was then aged under CO_2 free conditions for 18 months. Prior to analysis the sample was passed through a 0.45 μm Nylon filter and U(VI) was found to pass through the filter. SAXS data were collected on the I22 SAXS/WAXS beamline at the Diamond Light Source Ltd. using a Pilatus 2 M detector (Henrich et al., 2009). Data were collected with a 12 keV X-ray beam, using a camera lengths of 4 m (300 frames, 1 s/frame) and 10 m (60 frames, 10 s/frame). The collected data were averaged, background subtracted using a U(VI)-free calcite equilibrated YCL and merged into one data set. Data analysis was carried out using the Irena software macro for IgorPro 6.2 (Ilavsky and Jemian, 2009).

3. RESULTS AND DISCUSSION

3.1. U(VI) saturation and speciation

PHREEQC thermodynamic speciation and saturation calculations were carried out for 4.20 μM U(VI) in YCL and OCL solutions with and without calcite pre-equilibration (Table 2). These showed that both systems were predicted to be supersaturated with respect to several U(VI) phases. In OCL solutions, these phases were, in order of decreasing saturation, becquerelite ($Ca(UO_2)_6O_4(OH)_6 \cdot 8(H_2O)$), calcium uranate ($CaUO_4$), and calcium diuranate/calciouranoite (CaU_2O_7). By allowing the model to precipitate becquerelite out of solution, a final equilibrium U(VI) solution concentration of 1.7×10^{-2} μM was predicted. However, if calcium uranate was the solubility limiting phase, the final U(VI) concentration was predicted to be 2.07×10^{-5} μM. In YCL solutions, speciation modelling predicted supersaturation of calcium uranate and clarkeite ($Na_2U_2O_8$). Allowing calcium uranate to precipitate, the model predicted a final U(VI) concentration of 2.26×10^{-6} μM, at which point clarkeite was undersaturated. Including calcite equilibration in the model did not significantly alter the model predictions (Table 2). Solubility experiments were carried out in calcite pre-equilibrated OCL and YCL showed that after equilibration, 42.0 μM U(VI) was stable in solution (<0.45 μm nylon filter). This was in contrast to the PHREEQC calculations, which modelled the systems as significantly oversaturated.

The PHREEQC speciation calculations carried out at 4.20 μM U(VI) for solution speciation suggested that uranyl hydroxide species dominate aqueous speciation in both OCL and YCL systems (Table 3). In OCL, the dominant uranyl hydroxide species was $UO_2(OH)_3^-$ (86%), whereas, in YCL it was $UO_2(OH)_4^{2-}$ (97%). The $Ca_2UO_2(CO_3)_{3(aq)}$ species was predicted to account for only 0.19% of U(VI) speciation in OCL, although this was a much higher proportion than in YCL (Table 3). Free UO_2^{2+} accounts for a vanishingly small proportion of U(VI) in OCL and YCL (Table 3). Equilibrating OCL with calcite produced only minor changes in U(VI) speciation, with the most significant being the predicted presence of the $(UO_2)_2(CO_3)(OH)_3^-$ species (0.05%). In the YCL system, calcite equilibration had even less effect (Table 3). The proportions of $Ca_2UO_2(CO_3)_{3(aq)}$ in our experimental systems modelled using thermodynamic calculations were 0.19×10^{-11}% and 7.9×10^{-11}% for OCL and YCL systems, respectively. These values were orders of magnitude smaller in comparison to other published calcite-U(VI) studies (Geipel et al., 1997; Reeder et al., 2001; Elzinga et al., 2004), for example, Elzinga et al. (2004) calculated that the $Ca_2UO_2(CO_3)_3$ species accounted for >70% of all UO_2^{2+} in their pH 7.4 and 8.3 systems equilibrated with atmospheric carbon dioxide. The very much reduced abundance of $Ca_2UO_2(CO_3)_3$ in our experiments was due to both the very much lower carbonate concentrations, and elevated pH of the OCL and YCL systems. This has the potential to influence U(VI) behaviour in our systems, as the $Ca_2UO_2(CO_3)_{3(aq)}$ species has been demonstrated as key in the sorption of U(VI) to calcite surfaces (Reeder et al., 2001; Elzinga et al., 2004; Rihs et al., 2004).

Overall, the high pH of both OCL and YCL systems lead to speciation calculations being dominated by uranyl hydroxides ($UO_2(OH)_4^{2-}$ and $UO_2(OH)_3^-$), though the lower [OH^-] in OCL allowed for minor contributions from uranyl carbonates and the calcium uranyl triscarbonate species. In both YCL and OCL, the modelling suggested that U(VI) was supersaturated with respect to various U(VI) phases, although experimentally 42.0 μM U(VI) was stable in solution over extended periods (as defined by filtration through a 0.45 μm nylon filter).

3.2. Sorption experiments

Batch U(VI) experiments were carried out in both YCL and OCL systems with varying solid to solution ratios and U(VI) concentrations. Initial experiments were carried out at ultra-trace concentrations (5.27×10^{-5} μM; 10 Bq mL^{-1}) using a ^{232}U tracer to ensure undersaturation with respect to U(VI) oxyhydroxide phases. However, even with the use of an ultra-trace U(VI) spike, the systems were still predicted to be supersaturated with respect to calcium uranate (saturation index 0.84 (OCL) and 0.83 (YCL)) and calcium uranate like precipitates have been observed in high pH cement phase (Tits et al., 2011; Macé et al., 2013). Interestingly, in YCL systems, no removal of U(VI) from solution (⩽0.45 μm nylon filter) in control experiments without calcite present was observed (Bots et al., in press). The changing ^{232}U(VI) concentrations with respect to time for both YCL and OCL are shown in Fig. 1. In both systems, U(VI) removal took place over 675 h and after this time the system had reached apparent equilibrium. The

Table 2
PHREEQC calculated saturation indices (SI*) for supersaturated U(VI) phases at 4.20 μM in YCL and OCL with and without calcite equilibration.

Phase	YCL SI*	Calcite equilibrated YCL	OCL	Calcite equilibrated OCL
UO_4Ca (cr)	6.73	7.27	5.68	5.73
Clarkeite	3.60	3.60		
$U_2O_7Na_2$ (s)	3.40	3.40		
$CaU_2O_7{:}3H_2O$ (cr)	0.11	0.64	2.55	2.59
Becquerelite (nat)			14.3	14.3
Becquerelite (syn)			2.85	2.80

* SI is the saturation index $\left(\log \frac{\text{ion activity product}}{\text{solubility product}}\right)$.

Table 3
PHREEQC calculated U(VI) speciation (4.20 μM) as fractional composition in YCL and OCL with and without calcite equilibration.

Species	YCL	With calcite	OCL	With calcite
$UO_2(OH)_4^{2-}$	0.97	0.97	0.02	0.02
$UO_2(OH)_3^-$	0.03	0.03	0.86	0.79
$UO_2(OH)_2$	1.19×10^{-7}	1.2×10^{-7}	3.3×10^{-3}	2.9×10^{-3}
$UO_2(CO_3)_3^{4-}$		1.2×10^{-10}		1.8×10^{-4}
$(UO_2)_3(OH)_7^-$	1.47×10^{-12}	1.5×10^{-12}	0.04	0.03
$Ca_2UO_2(CO_3)_{3(aq)}$		7.9×10^{-13}		1.9×10^{-3}
$(UO2)_2(CO_3)(OH)_3^-$		6.8×10^{-13}		0.05
$CaUO_2(CO_3)_3^{2-}$		4.6×10^{-13}		9.2×10^{-5}
$UO_2(CO_3)_2^{2-}$		2.3×10^{-13}		4.5×10^{-5}
$UO_2(OH)^+$	6.6×10^{-14}	6.7×10^{-14}	8.6×10^{-7}	7.2×10^{-7}
$UO_2(CO_3)_{(aq)}$		2.2×10^{-16}		5.3×10^{-7}
UO_2^{2+}	4.3×10^{-22}	4.3×10^{-22}	5.3×10^{-12}	4.3×10^{-12}
$(UO_2)_3(OH)_5^+$	1.7×10^{-22}	1.2×10^{-22}	1.7×10^{-6}	1.1×10^{-6}
$(UO_2)_4(OH)_7^+$	3.8×10^{-28}	3.8×10^{-28}	1.5×10^{-7}	8.5×10^{-8}

proportion of U(VI) removed from solution in YCL at equilibrium was $71 \pm 4\%$; $27 \pm 5\%$; and $6 \pm 4\%$ for the 1:10, 1:50, and 1:500 solid to solution ratios, respectively. The proportion of U(VI) removed from solution in OCL at equilibrium was $60 \pm 0.9\%$; $30 \pm 5\%$; and $1 \pm 4\%$, for the 1:10, 1:50 and 1:500 systems, respectively (tabulated K_d values are available in the supporting information; Table S1). The geochemical modelling predicted that anionic uranyl hydroxide species (e.g. $UO_2(OH)_4^{2-}$, $UO_2(OH)_3^-$) dominated in these systems and that the concentrations of free $UO_{2(aq)}^{2+}$ and other cationic U(VI) species were vanishingly small. Calcite has a point of zero charge ranging from 8 to 9.5, depending on the exact solution composition and sample history (Somasundaran and Agar, 1967). Therefore, the calcite surface would be carrying a negative charge in both OCL and YCL systems. Given this and the predicted aqueous speciation, it was unlikely that the observed sorption was due to outer sphere complexation in either YCL or OCL and binding was probably dominated by inner sphere interactions.

A sorption model was developed to describe U(VI) sorption kinetics in both OCL and YCL ultra-trace systems. The model was parameterised using the data for the 1:10 systems, and it was then used to predict U(VI) removal from solution with respect to time in the 1:50 and 1:500 systems (Fig. 1). The OCL and YCL data were fitted separately to give rate constants (Eq. (1)) of $k_1 = 1.78 \times 10^{-6}$ L mol^{-1} s^{-1} and $k_2 = 7.50 \times 10^{-7}$ s^{-1} in YCL and $k_1 = 8.20 \times 10^{-7}$ L mol^{-1} and $k_2 = 5.12 \times 10^{-7}$ s^{-1} in OCL. The predictions for the 1:50 and 1:500 systems showed a good fit to the experimental data in the YCL and OCL systems (Fig. 1). The model was then used to predict removal from solution at equilibrium successfully with respect to solid to solution ratio (Fig. 2). Additional experiments were carried out with higher solid to solution ratios (1:2, 1:5) and were used to validate the sorption model by

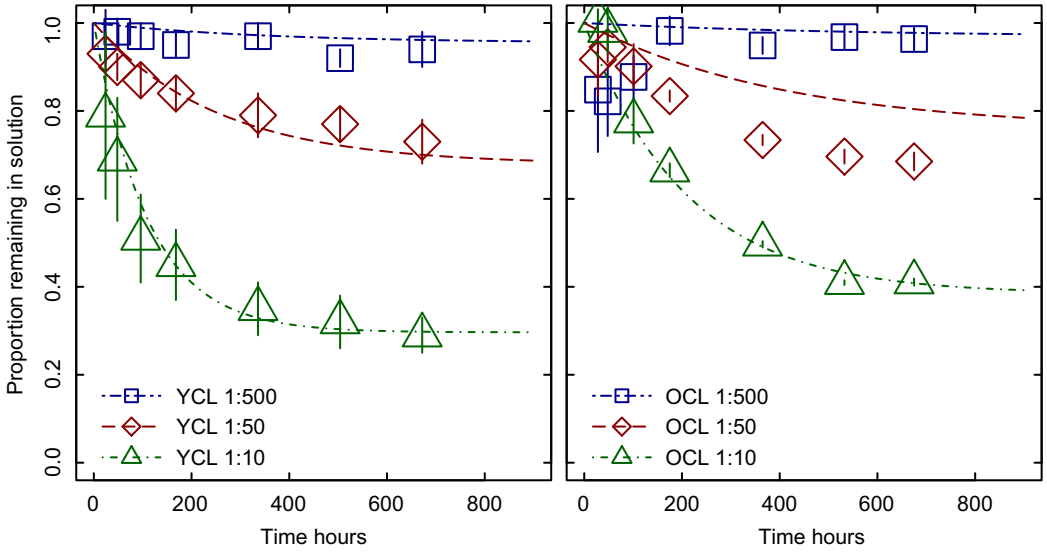

Fig. 1. Fraction of U(VI) (5.27×10^{-5} μM) remaining in solution versus contact time with calcite as a function of solid to solution ratio. Lines represent model predictions (calibrated with the 1:10 data set only). Error bars are 1σ of five replicates.

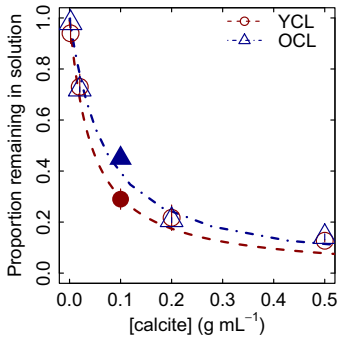

Fig. 2. Fraction of U(VI) (5.27×10^{-5} μM) remaining in solution at equilibrium versus calcite concentration. Symbols represent experimental data, lines represent predictions calculated using the sorption model. Only the filled triangle and circle data points (0.1 g mL^{-1} calcite) were used in fitting; hollow points are for comparison to the model. Error bars are 1σ from five replicates.

successfully predicting U(VI) concentration at solid to solution ratios much higher than the 1: 10 system (Fig. 2). These higher solid loading systems reflect more realistic ratios for transport in the subsurface where the solid will be present in excess. The sorption model was able to describe U(VI) behaviour at 5.27×10^{-5} μM across a wide range of solid solution ratios and this suggested that true surface complexation was occurring in these experiments. Unfortunately, there are no adsorption rate data for uranyl sorption to calcite surfaces available in the literature. However, the calculated adsorption rates in this study were slow compared to uranyl sorption on to other mineral phases such as goethite (Missana et al., 2003). In addition, in other uranium studies with calcite the authors typically allowed no more than a few days for the systems to reach a steady state before analysis (Rihs et al., 2004; Elzinga et al., 2004), which suggests that these high pH systems exhibit slower kinetics than would be expected. This is discussed in more detail below.

In order to explore uranium behaviour across a range of concentrations relevant to intermediate level waste disposal where U(VI) will be a significant component of wastes, batch sorption experiments at higher concentrations (0.42–42.0 μM) were carried out in YCL and OCL. In experiments with 42.0, 21.0 and 4.20 μM U(VI) YCL solutions, no statistically significant removal of uranium (<0.45 μm) was observed over a period of 18 months and over a range of solid to solution ratios (1:10, 1:50, and 1:500). At these concentrations, thermodynamic speciation modelling predicted that the YCL solution was significantly oversaturated with respect to calcium uranate (SI = 7.27) yet the U(VI) remained <0.45 μm filterable, probably due to colloid formation (Bots et al., in press). In the OCL experiments with 4.20, 2.10, 0.42 μM U(VI) OCL solutions there was significant U(VI) removal (<0.45 μm) from solution in all cases by 912 h (Fig. 3). At 4.20 μM U(VI), 87.3 ± 0.5%, 89.1 ± 0.5% and 99.9 ± 0.7% removal took place in the 1:10, 1:50 and 1:500 systems, respectively by 912 h. This trend continued at 2.10 μM U(VI), with 76.8 ± 6.5%, 88.3 ± 0.8% and 49.3 ± 17.4% removed for the 1:10, 1:50 and 1:500 systems by 912 h. However, at

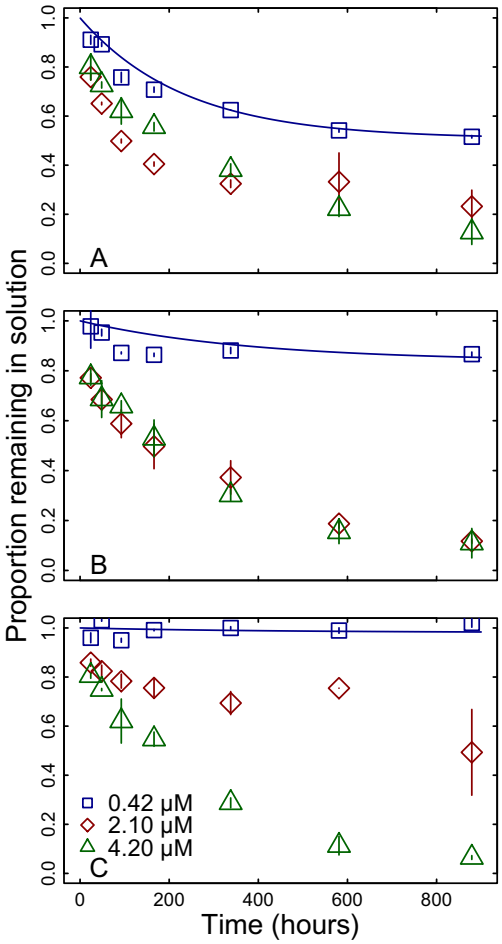

Fig. 3. Fraction of U(VI) (0.42–4.20 μM) remaining in OCL solution versus contact time with calcite as a function of solid to solution ratio (1:10 (A), 1:50 (B), 1:500 (C)). Lines represent predictions from the kinetic model for the 0.42 μM data calculated from the 1:10 data set with rate constants $k_1 = 1.78 \times 10^{-6}$ L mol^{-1} s^{-1} and $k_2 = 1.23 \times 10^{-6}$ s^{-1}. Error bars are 1σ of three replicates.

the lowest U(VI) concentration (0.42 μM), removal was reduced for all solid to solution ratios compared to the higher concentrations: removal of 48.5 ± 1.7%, 13.4 ± 0.8%, and 0.90 ± 0.5% U(VI) was observed, in the 1:10, 1:50, and 1:500 systems, respectively (K_d values are available in the supporting information; Table S1), by 912 h. In the 4.20 and 2.10 μM U(VI) OCL systems, removal did not appear to depend on solid to solution ratio, with consistently high removal. By contrast, in 0.42 μM U(VI) OCL solutions removal from solution appeared to be directly related to the solid to solution ratio (Fig. 3). Control samples without calcite present showed no U(VI) removal (<0.45 μm) at all concentrations (data not shown). The enhanced U(VI) removal from solution observed in the high U(VI) systems (4.20, 2.10 μM) in comparison to the 0.42 μM system, where the sorption model satisfactorily predicted behaviour, does not fit with a surface complexation mechanism which would be limited by the number of surface binding sites. Therefore, in the 4.20 and 2.10 μM

systems, U(VI) removal most likely involved a surface mediated precipitation mechanism. This precipitation did not take place in the no calcite experiments and clearly required the calcite surface. This is consistent with removal driven by the precipitation of various U(VI) phases observed by past workers, mainly oxyhydroxides and carbonates, although under different pH and carbonate concentrations to these studied here (Carroll et al., 1992; Geipel et al., 1997; Elzinga et al., 2004; Schindler and Putnis, 2004). However, in our experiments, removal occurred at lower U(VI) concentrations than reported elsewhere. This is probably due to the high pH and low carbonate concentrations in our study, which were aimed at deep disposal conditions. The sorption model was applied to the 0.42 μM U(VI) OCL data and was parameterised using the data from the 1:10 systems. This was then used to predict U(VI) removal from solution with respect to time in the 1:50 and 1:500 systems (Fig. 3). The OCL data gave rate constants (Equation (1)) of $k_1 = 1.78 \times 10^{-6}$ L mol^{-1} s^{-1} and $k_2 = 1.23 \times 10^{-6}$ s^{-1}. The predictions for the 0.42 μM U(VI) 1:50 and 1:500 systems provided a satisfactory fit for the experimental data (Fig. 3) and thus supported a surface complexation mechanism for this lowest U(VI) concentration experiment. The difference in rates measured in the 0.42 μM and the ultra-trace (5.2×10^{-5} μM) systems may suggest that multiple binding sites are available for U(VI) at the calcite surface, which is consistent with the literature (Elzinga et al., 2004). The kinetics of U(VI) removal were slow across all systems. Interestingly, all experiments were predicted to be supersaturated with respect to calcium uranate, even at low concentrations (5.27×10^{-5} μM) and the observed slow kinetics may be explained by U(VI) being speciated as calcium uranate colloids. Any U(VI) that was present in the form of a colloid would be unable to interact with the calcite surface. The small fraction of U(VI) that is truly dissolved in solution would be free to interact and sorb to the calcite surface. In a static system, this would indeed mean that the system rapidly reaches equilibrium. However, if the colloidal population were undergoing a constant, slow dissolution/recrystallisation process, through re-equilibration the fraction of free U(VI) truly dissolved in solution would be replenished. This would lead to a gradual increase in the fraction of U(VI) associated with the calcite surface and a decrease in solution concentrations.

Batch sorption experiments showed that in YCL, U(VI) showed little reactivity with the calcite surfaces unless the U(VI) concentration was very low. However, in OCL U(VI) exhibited dynamic behaviour with a surface complexation taking place at lower concentrations (⩽0.42 μM). Interestingly, at higher U(VI) concentrations (>0.42 μM), the relationship between total surface area and observed U(VI) removal was no longer present, which strongly supported a surface mediated precipitation process. This is in contrast to studies carried out at pH between 7 and 9 that indicate surface complexation is a key driver of U(VI) removal by calcite at lower concentrations (Elzinga et al., 2004; Reeder et al., 2004; Rihs et al., 2004) and that at elevated concentrations, precipitation is also possible (Carroll et al., 1992; Geipel et al., 1997; Elzinga et al., 2004; Schindler and Putnis, 2004). Interestingly, at circumneutral pH, the switch between surface complexation and precipitation reactions occurs at much higher U(VI) concentrations than our high pH experiments with, for example, surface complexation dominating at <500 μM U(VI) and with precipitation significant at >500 μM U(VI) in one example (Elzinga et al., 2004).

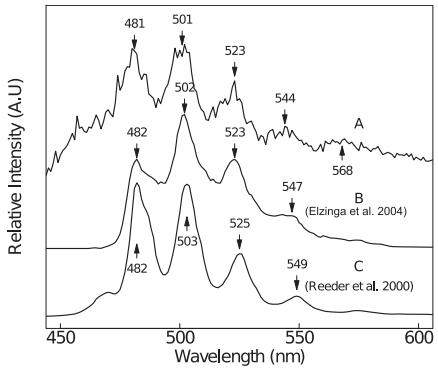

Fig. 4. (A) An ungated luminescence spectrum collected from the OCL 0.21 μM U(VI)–calcite sample following 250 nm excitation. (B) A luminescence spectrum of a U(VI)–calcite surface complex sample (5 μM U(VI), pH 7.4) following 420 nm excitation from Elzinga et al. (2004). (C) Luminescence spectrum (293 K) of a liebigite ($Ca_2UO_2(CO_3)_3$) standard following 420 nm excitation (Reeder et al., 2000).

3.3. OCL luminescence spectroscopy

To investigate the speciation of U(VI) associated wit h the calcite solid in the OCL systems, a series of

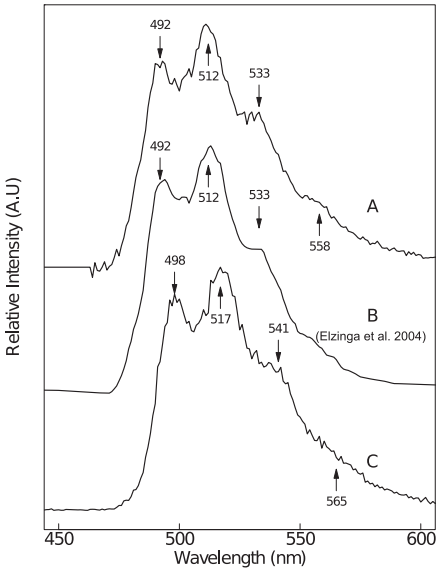

Fig. 5. (A) An ungated luminescence spectrum collected from the 0.42 μM U(VI) OCL calcite sample following 250 nm excitation. (B) A 'short gate' (0.05–0.1 ms) spectrum of 100 μM U(VI) sorbed onto calcite following 420 nm excitation from the literature (Elzinga et al., 2004). (C) Ungated luminescence spectrum collected from U(VI) incorporated into calcite standard following 250 nm excitation.

luminescence spectra taken at 77 K were collected from calcite samples reacted with 0.21, 0.42, 2.10 and 4.20 μM U(VI) OCL solutions (1:50 solid to solution ratio) and these data were compared with literature values and standards. Following excitation at 250 nm, the emission spectrum recorded for the 0.21 μM sample exhibited a vibrationally resolved structure despite a low signal to noise ratio (Fig. 4A). The emission maximum was centred at 501 nm and the estimated E_{0-0} transition at 20,790 cm^{-1}. The kinetic traces were fitted with biexponential decay kinetics, indicative of the presence of two distinct emissive species and the radiative lifetimes were calculated as 736 ± 12 μs (55%) and 1290 ± 20 μs (45%) (501 nm detection; Table S2). The fact that the lifetime of the second emissive species was considerably longer that of the first component used in the kinetic fitting model suggests that the uranyl(VI) ion is in an environment where there are fewer non radiative decay processes operating. This is likely to be due to loss of a carbonate/water ligand(s), which are known to quench the excited electronic state of uranyl (Natrajan, 2012). These data are remarkably similar to the results of Elzinga et al. (2004) for a calcite sample reacted at pH 8.3 with a 5 μM U(VI) solution (Fig. 4B) and for liebigite (Reeder et al., 2000; Fig. 4C) although no lifetime data were reported in these studies. This suggests that, in our study, a liebigite-like $Ca_2UO_2(CO_3)_3$ surface complex was forming at low U(VI)-concentrations.

Luminescence data (Fig. 5A) were also collected for a 0.42 μM U(VI) reacted calcite sample following 250 nm excitation at 77 K. This spectrum exhibited an emission maximum at 512 nm, an apparent E_{0-0} transition of 20,330 cm^{-1} and less resolved vibrational fine structure when compared to the 0.21 μM system. A double exponential fit of the luminescence decay profile gave lifetimes of 141 ± 2 μs (32%) and 515 ± 8 μs (68%) (500 nm detection), which were reduced in comparison to the 0.21 μM data. This spectrum resembled the data collected for the U(VI)–calcite coprecipitate standard but the emission maximum values were red shifted by approximately 7 nm (Fig. 5C; Table S2). In addition, the 0.42 μM spectrum closely matched a 'short gate' (0.05–0.10 ms) 100 μM sample reported by Elzinga et al. (2004) (Fig. 5B) and the radiative lifetimes were considerably shorter than those measured for the 0.21 μM sample suggesting the uranyl(VI) ion had undergone chemical transformation. With this information, we propose that the 0.42 μM spectrum collected in this study represents a second U(VI)–calcite surface coordination environment. Given that the 0.42 μM spectrum was collected ungated, it suggests that in our OCL system, this species was more abundant compared to the experiments of Elzinga et al. (2004). Our work was carried out in low carbonate conditions, in contrast to other studies which have been carried out in equilibration with atmospheric carbon dioxide (Carroll et al., 1992; Elzinga et al., 2004; Schindler and Putnis, 2004) or even with co-addition of carbonate (Elzinga et al., 2004).

In OCL at 4.20 μM U(VI), the highest concentration luminescence experiment, the spectrum showed the presence of two species, with peaks at 524, 543 and 567 nm (and minor peaks at 482, 505 nm; Fig. 6A). The spectrum

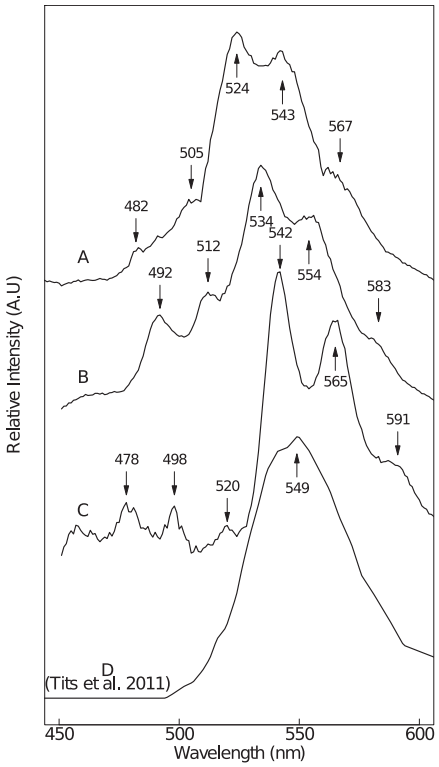

Fig. 6. (A) An ungated luminescence spectrum from a 4.20 μM U(VI) OCL calcite sample following 250 nm excitation. (B) Ungated luminescence spectrum from a 2.10 μM U(VI) OCL calcite sample following 250 nm excitation. (C) Ungated luminescence spectrum from an (84.0 μM) OCL U(VI) precipitate following 250 nm excitation. (D) Ungated luminescence spectrum a calcium uranate sample following 420 nm excitation from the literature (Tits et al., 2005).

collected for the 2.10 μM U(VI) sample was similar to the 4.20 μM U(VI) sample, but the emission bands were red shifted by approximately 10 nm (Fig. 6B), suggestive of an elongation of the uranyl bond in this species (Redmond et al., 2011). Additionally, the spectra were vibrationally broadened compared to the lower uranyl loading samples. This is indicative of a lower formal bond order of the uranyl unit and a significantly altered electronic (and therefore chemical) environment in comparison with the lower U(VI) concentration systems. The 525–575 nm region in both 4.20 and 2.10 μM samples was broadly similar to the spectrum collected from a U(VI) phase precipitated by an oversaturation experiment with 84.0 μM U(VI) OCL solution (Fig. 6C) and it also corresponds well to the calcium uranate spectrum reported by Tits et al. (2005) (Fig. 6D) and various other U(VI) phases, such as schoepite and becquerelite (Wang et al., 2008). A triple exponential fit of the luminescence decay was required for the 2.10 and 4.20 μM samples, suggesting that U(VI) was hosted in several different environments and highlighting the complicated speciation of uranyl in these samples. The lifetimes calculated for the 2.10 μM system were 26 ± 1 μs (6%), 94 ± 3 μs (35%) and 422 ± 11 μs (57%) (512 nm detection), whereas for 4.20 μM they were slightly shorter at 22 ± 1 μs (13%), 105 ± 4 μs (6%), and

319 ± 11 μs (36%) (503 nm detection). The additional short lived species (22 μs) were in broad agreement with the lifetimes calculated for the 84.0 μM U(VI) OCL precipitate (23 ± 1 μs (35%) and 75 ± 1 μs (53%) μs; 542 nm detection). The extra component to the lifetime fits and the emergence of the red shifted feature, strongly suggested that the spectra for the 2.10 and 4.20 μM samples were a combination of different species with both a U(VI) solid phase and a U(VI) surface complex present. The relative intensities of the minor peaks (492, 512 nm), which we assume are indicative of the surface complex, were greater in the 2.10 μM U(VI) sample compared to the 4.20 μM U(VI) sample. Qualitatively, these data indicated that the surface complex component of the spectra was more significant at lower U(VI) concentrations. It is interesting to note that there was an apparent red shift in the luminescence data for the solids as the U(VI) concentration increased. This has been reported previously for calcium uranate solids (Blasse, 1976) and is indicative of a reduction in the uranyl bond order as the form of the uranium species changes.

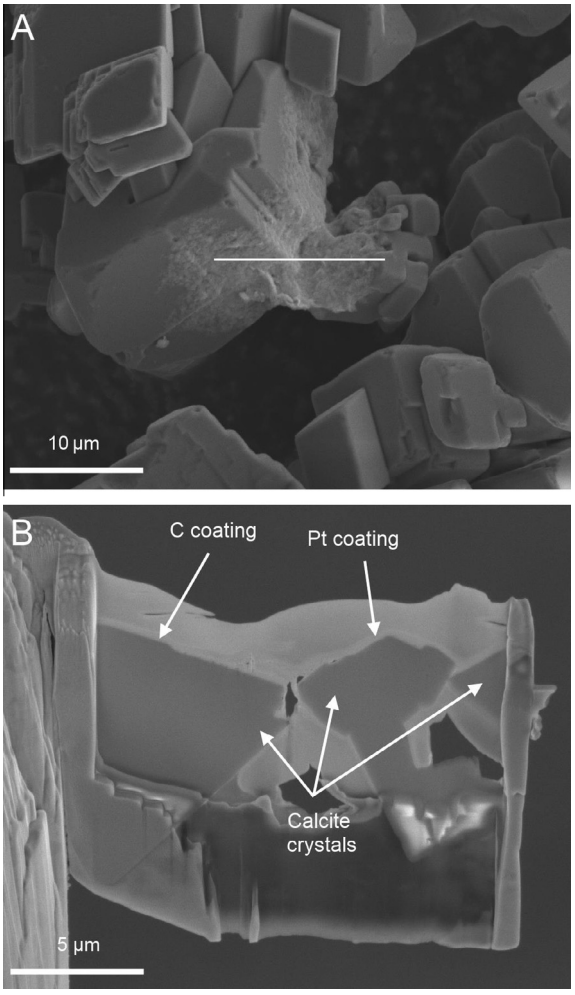

Fig. 7. (A) Backscattering electron image of calcite crystal coated with an electron dense material, lighter areas indicate higher electron density. The white line indicates the area in which the TEM thin section was prepared. (B) SEM image of the calcite thin section (approximately 10 μm wide and 100 nm at its thinnest).

The luminescence data suggest a complex, concentration dependent U(VI) behaviour in the OCL system. At the lowest loadings (0.21 μM), a liebigite-like U(VI)–calcite surface complex was identified. At 0.42 μM U(VI), a second as yet unidentified surface complex dominated the luminescence spectrum. At higher concentrations a different species which was red shifted with respect to the surface complexes appeared to grow in with increased concentration, consistent with the formation of a U(VI) solid phase.

3.4. OCL electron microscopy

In order to characterise the OCL U(VI) surface mediated precipitate further and to explore the interface between it and the calcite solid, a sample from the 4.20 μM U(VI) OCL (1:50) calcite batch sorption experiment was analysed using electron microscopy. SEM images showed crystals (2–20 μm) with the *rhombohedral* morphology typical of calcite. Backscattering electron imaging (Z constant imaging) showed that the majority of crystals did not have a visible secondary phase, but several crystals were coated with a phase with higher average atomic number, which shows up as brighter regions on the image (Fig. 7A). A section (10 μm long × 100 nm thick) was then prepared using a FIB mill in order to examine both the secondary phase and the interface between it and the calcite solid using TEM (Fig. 7B).

Elemental mapping via TEM-EDX analysis was carried out at the interface between the calcite and the secondary phase (Fig. 8). The mapping indicated a uranium rich coating on the calcite surface, with a thickness ranging from approximately 10 to 100 nm. Within the limits of analysis for EDX, there was no indication of any uranium in the uppermost layer of the calcite structure (approximately 300 nm from interface, see supporting information; Figure S2). Further EDX analysis of the uranium-rich surface coating showed it contained uranium, calcium and oxygen. The peaks for all other elements are related to either the support grid (Cu and C) or the FIB process (Ga, see

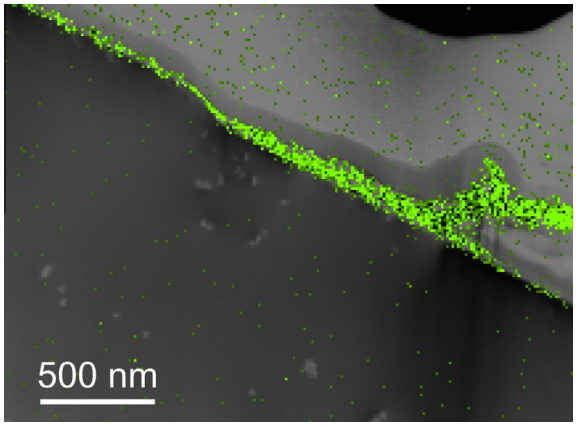

Fig. 8. Energy dispersive X-ray elemental map overlaid onto high angle annular dark-field image (z contrast) of the calcite surface showing a thin uranium rich (green) coating. (For interpretation of the references to colour in this figure legend, the reader is referred to the web version of this article.)

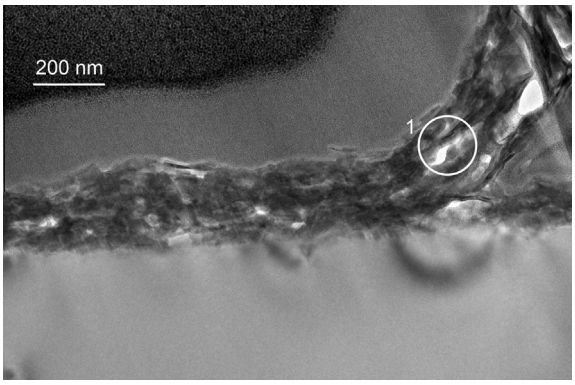

Fig. 9. High magnification image of a calcite surface coated with a uranium containing phase. The selected area electron diffraction image (Fig. 11) was collected from site 1.

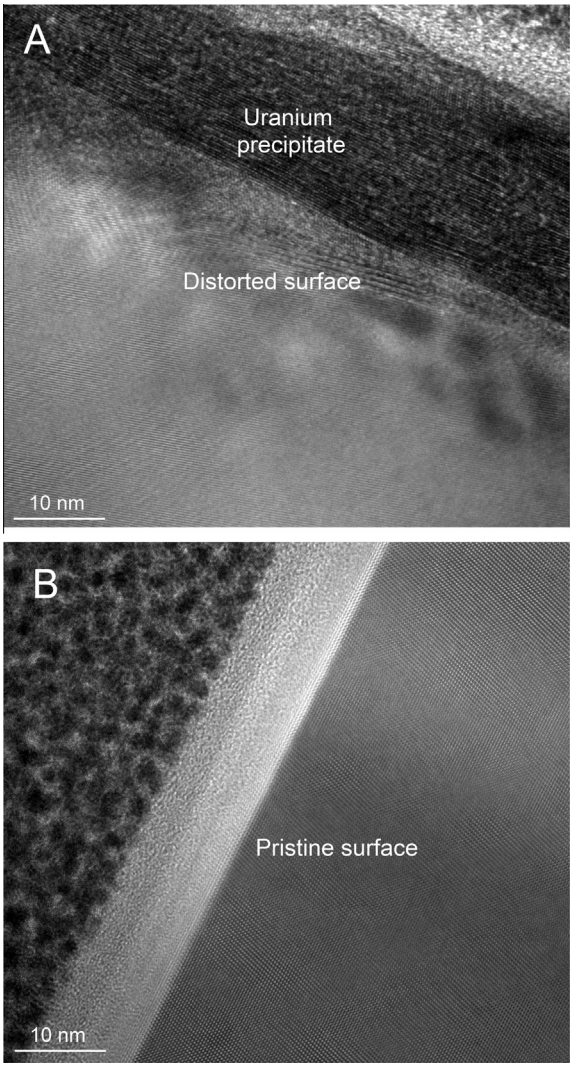

Fig. 10. (A) High magnification TEM image of the uranium containing phase and a distorted calcite surface. (B) High magnification TEM image of a 'pristine' calcite surface.

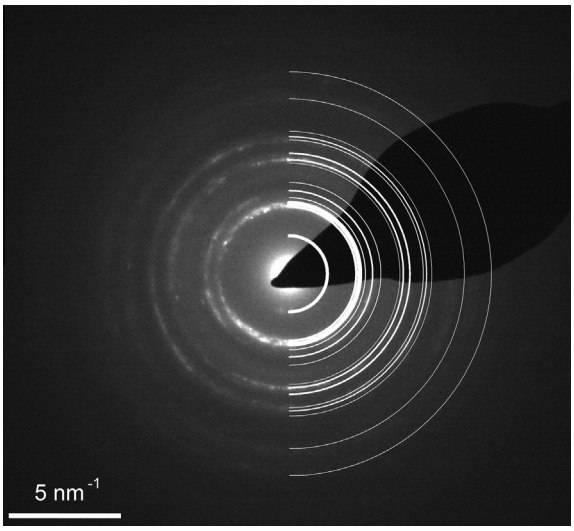

Fig. 11. Selected area electron diffraction image collected from U(VI) precipitate (Fig. 9, site 1) overlain with powder diffraction data calculated from crystallographic data for calcium uranate (Zachariasen, 1948).

supporting information; Figure S3). This suggests that the secondary phase is a U/Ca phase.

Further TEM analysis of the uranium–calcite interface showed that the U(VI)-bearing precipitate consisted of elongated nanoparticles, 10–200 nm in length and approximately 20 nm in thickness (Fig. 9). High resolution images of the particles show lattice fringes indicating the particles are nano-crystalline. The individual crystals were orientated roughly parallel to the calcite surface, as shown in Fig. 10A. Interestingly, the pristine calcite surface with no secondary phase showed little distortion and a clean termination of the calcite lattice (Fig. 10B). However, the uranium coated surface showed indications of distortion and an uneven surface, with the lattice terminating in multiple orientations (Fig. 10 B). This suggested that the formation of the uranium solid had altered the calcite surface, either during precipitation or though interaction with the solid once it had formed.

In order to identify the U(VI) rich precipitate, SAED patterns were collected from several sites with a representative example, site 1, shown in Fig. 9. This showed the presence of diffraction rings which is indicative of the crystallites being oriented in multiple directions (Fig. 11). The PHREEQC saturation calculations suggested that becquerelite ($Ca(UO_2)_6O_4(OH)_6{\cdot}8(H_2O)$) was a likely candidate for the precipitate, but the crystallographic data for this phase (Piret-Meunier and Piret, 1982) was a poor fit to the SAED data (see supporting information; Figure S4). Likewise, it was a poor match for other candidate phases, such as schoepite (see supporting information; Figure S5). However, the pattern was a good match for calcium uranate (Fig. 11; Zachariasen, 1948) and this is consistent with the composition of the phase as determined by EDX. Calcium uranate phases such as vorlanite (cubic $CaUO_4$; Galuskin et al., 2011) and calcium diuranate/calciouranoite ($Ca_2U_2O_7$; Rogova et al., 1974) produce very similar

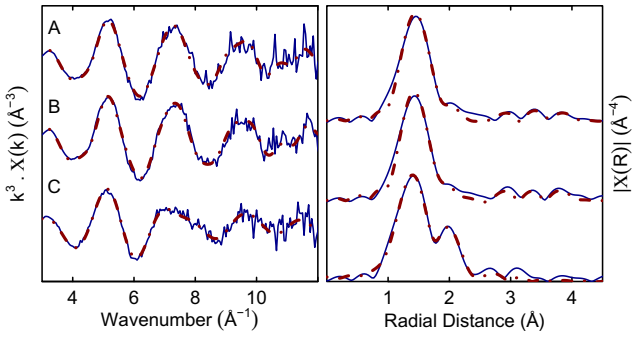

Fig. 12. k^3-weighted χ functions with Fourier transforms for: (A) 0.10 g calcite reacted with 50 mL 21.0 μM U(VI) OCL solution; (B) 0.10 g calcite reacted with 50 mL 42.0 μM U(VI) OCL solution; (C) U(VI) coprecipitated with calcite standard. Solid lines represent experimental data while dashed lines are the fits using the parameters listed in Table 4.

diffraction patterns (see supporting information; Figure S6). Therefore, we have putatively identified the solid U(VI) phase present at the mineral interface in this system as calcium uranate. This is in contrast to other studies which have reported the formation of solid phases, such as schoepite (Schindler and Putnis, 2004) and uranyl hydroxide (Geipel et al., 1997) in calcite sorption experiments, although it is noteworthy that these experiments were at lower pH values and in equilibrium with atmospheric CO_2. A SAED pattern from the calcite solid (see supporting information; Figure S7) was confirmed as a single crystal of calcite.

3.5. OCL extended X-ray absorption fine structure spectroscopy

Due to the low U(VI) concentrations in many experiments, only a select set of samples with low solid to solution ratios, and high U(VI) uptake (21.0 and 42.0 μM; 1:500) were suitable for EXAFS analysis. EXAFS spectra and corresponding Fourier transforms, including fits to the data, for these samples and a standard consisting of calcite coprecipitated with U(VI) are shown in Fig. 12.

The best fit to the EXAFS spectra from the coprecipitated U(VI) calcite standard indicated the U was bonded to 2 axial oxygens at 1.81 Å, and 6 equatorial oxygens at distances between 2.20 and 2.38 Å. In addition, there was a shell of 3 C atoms at 2.90 Å (Table 4). This is consistent with previous models for U(VI) incorporation into calcite

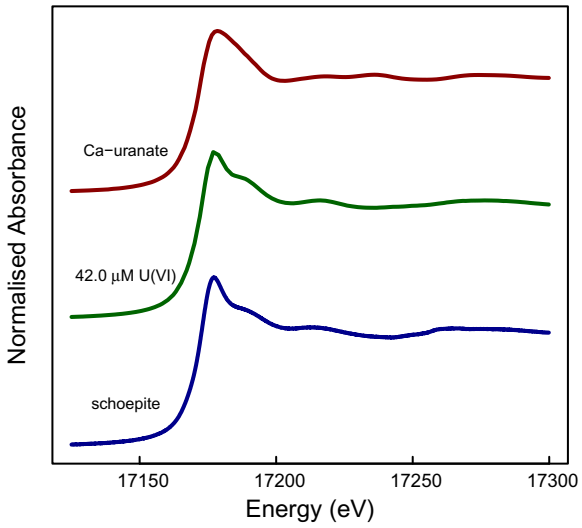

Fig. 13. Normalised XANES spectra for the U L_{III} edge of a 42.0 μM U(VI) reacted calcite sample (1:500) and Ca-uranate (Macé et al., 2013) and schoepite standards.

Table 4
EXAFS best fit parameters for U(VI)–calcite samples.

	42.0 μM (A)			21.0 μM (B)			Coprecipitated (C)		
	N	*R* (Å)	σ^2 (Å^2)	*N*	*R* (Å)	σ^2 (Å^2)	*N*	*R* (Å)	σ^2 (Å^2)
U–O_{ax}	2	1.81 ± 0.01	0.003 ± 0.001	2	1.81 ± 0.01	0.002 ± 0.001	2	1.78 ± 0.01	0.004 ± 0.001
U–O_{eq1}	2.5	2.23 ± 0.02	0.003 ± 0.002	2.5	2.23 ± 0.02	0.002 ± 0.001	2	2.20 ± 0.02	0.003 ± 0.001
U–O_{eq2}	2.5	2.40 ± 0.02	0.006 ± 0.004	2.5	2.40 ± 0.02	0.003 ± 0.002	4	2.38 ± 0.02	0.004 ± 0.001
U–C							3	2.90 ± 0.02	0.010 ± 0.004
U–U_1	1	3.65 ± 0.05	0.005 ± 0.004	1	3.66 ± 0.04	0.004 ± 0.004			
U–U_2	3	3.85 ± 0.05	0.011 ± 0.004	3	3.88 ± 0.05	0.013 ± 0.005			
$S0^2$		0.96			0.9			0.98	
ΔE0		1.72			2.2			−2.51	
Reduced χ^2		71			24.8			20.2	
R		0.012			0.011			0.007	

Coordination numbers for samples A and B were fixed to those found in becquerelite while sample C were fixed to those found in liebigite. A forward through absorber multiple scattering path was included for the axial oxygens in all systems.

which demonstrates that U(VI) incorporated into calcite has a similar coordination environment to a U(VI)–calcite surface complex (Elzinga et al., 2004). However the data collected for the U(VI) reacted calcite samples did not resemble the coprecipitated standard. Therefore, given this and previous data suggesting a surface mediated precipitate, the data were interpreted in the context of a U(VI) solid phase. The spectra are similar to those produced by various U(VI) oxyhydroxides in the literature (Catalano and Brown, 2004), however, the TEM data strongly supported the formation of a calcium uranate solid. It was not possible to fit the EXAFS data with a calcium uranate crystal structure (Zachariasen, 1948) without a significantly shorter "uranyl like" O_{ax} distance of 1.81 Å compared to the 1.97 Å found in the structure. In addition, the XANES spectrum for the 42.0 and 21.0 μM U(VI) reacted calcite samples did not resemble calcium uranate (Macé et al., 2013), and instead appeared closer to a "uranyl like" schoepite reference, which contained a shorter U–O_{ax} distance as demonstrated by the shoulder in the edge region (Fig. 13). Given that becquerelite ($Ca(UO_2)_6O_4(OH)_6{\cdot}8(H_2O)$) was predicted to be supersaturated in calcite equilibrated OCL, the EXAFS data were fitted using scattering paths and fixed coordination numbers taken from becquerelite crystallographic data (Burns and Li, 2002) which has a shorter O_{ax} distance than calcium uranate (Table 4). The U–O_{ax}–U scattering path was refined to a distance of 1.81 ± 0.01 Å and the five equatorial oxygens were fitted as two shells of oxygen atoms at 2.23 and 2.40 Å, with an occupancy of 2.5 each. This was consistent with becquerelite, which has 5 equatorial oxygen atoms at distances varying from 2.10 to 2.60 Å (Burns and Li, 2002). This offered a significant improvement over the single shell fit (>5% improvement in reduced χ^2, see supporting information; Table S3). A further two shells of uranium at 3.66 and 3.86 Å could also be fitted, which is again consistent with the becquerelite structure which has four uranium atoms at distances varying from 3.7 to 3.9 Å (Burns and Li, 2002). Interestingly, no calcium scatters were identified in the EXAFS modelling, most likely because of its relatively low mass and long distance from the absorber atom (4.20 Å). It is noteworthy that, while becquerelite crystallographic data were used in the calculation of the theoretical scattering paths and amplitudes, subtle differences between becquerelite and other uranium phases such as schoepite (Allen et al., 1996; Finch et al., 1996) would be difficult to distinguish with EXAFS spectroscopy. In summary, SAED data from this study suggested the formation of calcium uranate in the calcite systems at a U(VI) concentration of 4.20 μM. By contrast, EXAFS data from 21.0 and 42.0 μM U(VI)–calcite samples were modelled with a U(VI) phase with a shorter axial oxygen distance, best modelled as a uranyl oxyhydroxide mineral such as becquerelite. This suggested that the speciation changed between the 4.20 μM and the >21.0 μM systems, with calcium uranate dominating the samples at lower U(VI) concentrations (2.10 and 4.20 μM) and a uranyl oxyhydroxide precipitate dominating at ⩾4.20 μM and again highlighting the complexity of the system.

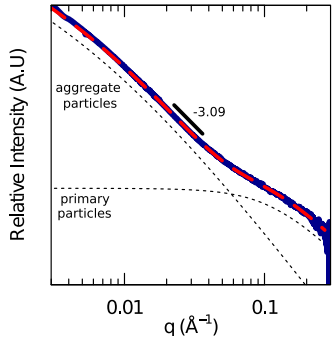

Fig. 14. SAXS data collected from a 42.0 μM U(VI) calcite equilibrated YCL solution, aged for 18 months. Solid line represents the experimental data, the dashed line the modelled intensity, and the dotted lines indicate the relative contribution of the two particle populations. The gradient of the Porod region was calculated as −3.09.

3.6. YCL small angle X-ray scattering

YCL batch sorption experiments suggested that U(VI) was stable in solution at elevated concentration (42.0 μM; <0.45 μm filtered) over an extended time, and had little affinity for the calcite surface. However, PHREEQC modelling suggested that the system was significantly supersaturated with respect to U(VI) oxyhydroxide and calcium uranate phases. This highlighted that U(VI) may be present as a stable colloidal phase unable to interact with the calcite surface. To explore this further, a 42.0 μM U(VI) calcite equilibrated YCL solution was aged for 18 months and the filtered solution was then analysed using SAXS. The SAXS data showed scattering above background (Fig. 14), indicating the U(VI) was present in a colloidal form.

The best fit to the SAXS data was achieved using a two particle population model: firstly, a spheroid population to represent primary particles; and secondly a population with an algebraic globule form factor (Reidy et al., 2001) which represent aggregates of the primary particles (Fig. 14 and Table 5). A best fit of the model against experimental data suggested the primary particles and aggregates had a radius of 7.6 ± 1.1 and 217 ± 24 Å, respectively (Table 5). The Porod slope for the larger particles was approximately −3 (Fig. 14), which suggests the particulates had surface fractal properties (Schmidt, 1991). The volume ratio of the primary particle to aggregates was 1.05. The SAXS data suggested that the U(VI) in the YCL systems was present as suspended nanoparticles. It is not possible to determine the chemical composition of the colloid population using SAXS, however, given the U(VI) saturation calculations (Table 2), calcium uranate is clearly a candidate. It is also not possible to determine the proportion of U(VI) present as a colloid using SAXS, however PHREEQC calculations suggest that, if the system were at equilibrium with calcium uranate, >99% of U(VI) would be present as a solid phase.

Table 5
Summary of fitted parameters in SAXS model.

	Radius (Å)	Polydispersity*	Volume ratio (Primary/Aggregate)
Primary particles	7.6 ± 1.1	0.62 ± 0.11	1.05
Aggregated particles	217 ± 24	1.05 ± 0.23	

* Log-normal distribution.

Table 6
Summary of mechanisms of U(VI) uptake to calcite solids in calcite-equilibrated OCL systems.

U(VI) concentration range	U(VI)–calcite mechanism
$\leqslant$0.42 μM	Surface complexation dominates removal, as demonstrated with batch data and kinetic modelling
<0.21 μM	Luminescence spectroscopy suggest a liebigite-like $Ca_2UO_2(CO_3)_3$ U(VI)–calcite surface complex as the primary binding site at low concentrations
$\geqslant$0.42 μM	Luminescence spectroscopy suggest a second U(VI)–calcite binding site exists, resembles spectrum from U(VI) coprecipitated with calcite
$\geqslant$2.10 μM	Surface mediated precipitation denominates removal. SAED data confirms calcium uranate solids dominate over sampling area. Surface complexation still likely to account for a fraction of U(VI) uptake
>21.0 μM	Surface mediated precipitation continues. XANES and EXAFS spectroscopy suggest U(VI) speciated as uranyl oxyhydroxide such as becquerelite or schoepite

3.7. U(VI) speciation and uptake mechanisms with pH: concentration and surface area

The data collected in this study demonstrate the complex behaviour of U(VI), with the mechanisms of interaction changing from surface complexation, to surface precipitation, to formation of a U(VI) colloidal phase depending on the cement leachate pH, amount of calcite, and U(VI) concentration (Table 6).

At low UVI concentrations in both the YCL ($[U(VI)] = 5.27 \times 10^{-5}$ μM) and OCL ($U(VI) = 5.27 \times 10^{-5}$ to 0.42 μM) systems, U(VI) removal could be directly related to the available surface area, and was successfully modelled assuming a surface complexation mechanism. Luminescence spectroscopy from a 0.21 μM U(VI) OCL reacted calcite sample suggested a liebigite-like $Ca_2UO_2(CO_3)_3$ surface complex identical to that reported by Elzinga et al. (2004). In contrast, the spectrum produced by a 0.42 μM U(VI) OCL reacted calcite sample was different, resembling a red-shifted U(VI)–calcite incorporated species and with similarities to spectra reported for U(VI) sorbed to the '-' steps of the calcite (1 0 4) surface (Elzinga et al., 2004). This species was interpreted as representing a second, surface binding site of lower U(VI) reactivity than the liebigite-like surface complex which was similar to the calcite incorporated species observed here and reported in the literature (Reeder et al., 2000; Elzinga et al., 2004). The identification of U(VI)–calcite surface complexation implies U(VI) removal may be reversible in some systems where the concentration is low. However, it is interesting to note the similarity between the second binding site and U(VI) incorporated into calcite is clearly worthy of further consideration.

In batch sorption experiments at higher U(VI) concentrations in OCL (2.10–42.0 μM) the relationship between U(VI) removal and calcite surface area broke down. This suggested a new regime where formation of a U(VI) precipitate occurred in agreement with other studies (Carroll et al., 1992; Geipel et al., 1997; Elzinga et al., 2004; Schindler and Putnis, 2004). Indeed, control experiments with calcite equilibrated solutions showed no removal of U(VI) upon filtration, suggesting a calcite surface induced reaction for U(VI) removal in the systems with mineral present. In addition, the luminescence data for higher U(VI) concentrations (2.10–4.20 μM U(VI) OCL) showed features which fit a variety of U(VI) solid phases (Tits et al., 2005; Wang et al., 2008). TEM analysis from a sample prepared with 4.20 μM U(VI) indicated that the surface phase was a calcium uranate. However, at $\geqslant$ 21 μM U(VI) loading, XAS suggested that the surface precipitate was a uranyl oxyhydroxide phase. Given the differences between the XAS (42.0 μM) and TEM data (4.20 μM), it is possible that the system is undergoing predominantly calcium uranate precipitation at lower concentrations, while uranyl oxyhydroxide phases dominate at higher concentrations. This is consistent with the fact that the increased U(VI) concentration significantly increases the saturation of becquerelite (uranyl oxyhydroxide) by approximately five units (see Supporting Information; Table S4).

In the pH 13.3 YCL system, U(VI) uptake (4.20–42.0 μM) by calcite was not observed over long time scales (18 months), and in the OCL system experiments were typically observed to have long equilibration times for metal uptake (>1 month). This was surprising as metal complexation to mineral surfaces normally displays fast kinetics with typical equilibration times between 24 and 28 h (Davis et al., 1987; Giammar and Hering, 2001; Rihs et al., 2004). Interestingly, SAXS analysis indicated that in YCL at high U(VI) concentrations, U(VI) was largely present as a stable colloidal phase over 18 months which had a primary particle radius of 7.6 Å. These data suggest that for the YCL system, stable colloidal phases will contribute the dominant species (>99%) of U(VI) present, presumably as one of the oversaturated phases predicted from the thermodynamic modelling and presumably explaining the poor reactivity of U(VI) at all but ultra-trace levels in the YCL system. Also, if a colloidal population

were present in the other OCL and low level YCL systems it could explain the slow kinetics of removal observed in experiments. The presence of colloidal U which is stable over year timescales in high pH systems, is a potentially significant finding (Porcelli et al., 1997; Wieland et al., 2004; Novikov et al., 2006)and clearly warrants further study in the context of uranium mobility under geological disposal conditions (Bots et al., in press).

4. CONCLUSIONS

At high pH in model cement leachate systems, U(VI) had several interaction mechanisms with calcite. At low concentrations ($\leqslant$0.42 μM), U(VI) removal was successfully modelled assuming a surface complexation reaction. Luminescence spectroscopy identified two distinct U(VI) surface binding sites at two different U(VI) concentrations (0.21 and 0.42 μM). At higher concentrations ($\geqslant$2.10 μM) experiments showed U(VI) removal via a surface mediated precipitation mechanism. This was confirmed by luminescence spectroscopy, which identified a U(VI) phase that corresponds well to various U(VI) solid phases, such as calcium uranate and becquerelite. Furthermore, a calcite crystal coated with a U(VI) solid phase in the 4.20 μM system was identified using TEM as calcium uranate. In experiments at high U(VI) concentrations, 21.0 and 42.0 μM, EXAFS spectroscopy successfully identified U–U scatters, indicative of a uranyl oxyhydroxide like solid phase.

For YCL systems, U(VI) showed no interaction with the calcite surfaces unless the concentration was very low (5.27×10^{-5} μM) and over a period of 18 months. Where U(VI) removal from solution was observed, the kinetics were slow relative to many metal ion uptake studies and experiments took a month and more to reach apparent equilibrium. Interestingly, despite the fact that U(VI) was stable in solution (<0.45 μm), the systems were predicted to be supersaturated with various U(VI)-bearing phases. Further characterisation using SAXS techniques confirmed that a U(VI) colloidal form was present in these solutions. These colloids consisted of aggregated and primary particles with a diameter of 217 ± 24 and 7.6 ± 1.1 Å, respectively.

Overall, these data demonstrate for the first time the complex nature of U(VI) interactions with calcite solids in hyperalkaline systems representative of young and aged cement leachates. They suggest that for the YCL system representative of early evolution within a GDF, calcite is likely to have limited impact on the mobility of U(VI). However, in OCL systems representative of an aged cementitious geological disposal facility, a complex set of mechanisms allows for significant U(VI) uptake by both surface complexation and surface mediated precipitation of U(VI) solid phases. Under these conditions, the capacity for U(VI) uptake by interactions with calcite is likely to increase with increasing U(VI) concentration and in direct contrast to circumneutral environments.

ACKNOWLEDGEMENTS

Kurt Smith was a Nuclear FiRST DTC student, funded by EPSRC (FIRST EP/G037140/1). This work was carried out as part of the Biogeochemical Gradients and Radionuclide Transport (BIGRAD) consortium, funded by NERC (NE/H007768/1) and with assistance from Louise S. Natrajan (an EPSRC Career Acceleration Fellow) and Adam N. Swinburne (an EPSRC funded postdoctoral researcher). We thank Diamond Light Source for access to beamline I22 (SM5975) and beamline B18 (SP7593) that contributed to the results presented here. The authors would like to thank Paul Lythgoe (geochemical analyses), Mike Ward (electron microscopy/FIB milling), John Waters (electron microscopy/BET analysis), Katie Law (radiochemical separations), Gareth Law and Tim Marshall (XAS data acquisition) for assistance in the preparation of this work. Kurt Smith and Nick Bryan would also like to thank NNL for support.

APPENDIX A. SUPPLEMENTARY DATA

Supplementary data associated with this article can be found, in the online version, at http://dx.doi.org/10.1016/j.gca.2014.09.043.

REFERENCES

Allen P. G., Shuh D. K., Bucher J. J., Edelstein N. M., Palmer C. E. A., Silva R. J., Nguyen S. N., Marquez L. N. and Hudson E. A. (1996) Determinations of uranium structures by EXAFS: Schoepite and other U(VI) oxide precipitates. *Radiochim. Acta* **75**, 47–53.

Bernhard G., Geipel G., Reich T., Brendler V. and Amayri S. (2001) Uranyl(VI) carbonate complex formation: Validation of the $Ca_2UO_2(CO_3)_{3(aq.)}$ species. *Radiochim. Acta* **89**, 511–518.

Blasse G. (1976) Nature of the luminescent centers in calcium uranate (Ca_3UO_6). *Solid State Commun.* **19**, 779–781.

Braney M. C., Haworth A., Jefferies N. L. and Smith A. C. (1993) A study of the effects of an alkaline plume from a cementitious repository on geological materials. *J. Contam. Hydrol.* **13**, 379–402.

Bots P., Morris K., Rosemary H., Law G., Mosselmans F., Brown A., Doutch J., Smith A. and Shaw S. (in press) Formation of stable uranium(VI) colloidal nanoparticles in conditions relevant to radioactive waste disposal. *Langmuir*.

Burns P. C. and Li Y. P. (2002) The structures of becquerelite and Sr-exchanged becquerelite. *Am. Mineral.* **87**, 550–557.

Carroll S. A., Bruno J., Petit J. C. and Dran J. C. (1992) Interactions of U(VI), Nd and Th(VI) at the calcite-solution interface. *Radiochim. Acta* **58–9**, 245–252.

Catalano J. G. and Brown G. E. (2004) Analysis of uranyl-bearing phases by EXAFS spectroscopy: Interferences, multiple scattering, accuracy of structural parameters, and spectral differences. *Am. Mineral.* **89**, 1004–1021.

Curti E. (1999) Coprecipitation of radionuclides with calcite: Estimation of partition coefficients based on a review of laboratory investigations and geochemical data. *Appl. Geochem.* **14**, 433–445.

Davis J. A., Fuller C. C. and Cook A. D. (1987) A model for trace metal sorption processes at the calcite surface. Adsorption of Cd2+ and subsequent solid solution formation. *Geochim. Cosmochim. Acta* **51**, 1477–1490.

DEFRA (2008) Managing radioactive waste safely: A framework for implementing geological disposal. Department for Environment Food and Rural Affairs, 2008.

Dong W., Ball W. P., Liu C., Wang Z., Stone A. T., Bai J. and Zachara J. M. (2005) Influence of calcite and dissolved calcium on uranium(VI) sorption to a Hanford subsurface sediment. *Environ. Sci. Technol.* **39**, 7949–7955.

Doudou S., Vaughan D., Livens F. and Burton N. (2012) Atomistic simulations of calcium uranyl(VI) carbonate adsorption on calcite and stepped-calcite surfaces. *Environ. Sci. Technol.* **46**, 7587–7594.

Dow C. and Glasser F. P. (2003) Calcium carbonate efflorescence on Portland cement and building materials. *Cement Concrete Res.* **33**, 147–154.

Elzinga E. J., Tait C. D., Reeder R. J., Rector K. D., Donohoe R. J. and Morris D. E. (2004) Spectroscopic investigation of U(VI) sorption at the calcite-water interface. *Geochim. Cosmochim. Acta* **68**, 2437–2448.

Finch R. J., Cooper M. A., Hawthorne F. C. and Ewing R. C. (1996) The crystal structure of schoepite, $(UO_2)_8O_2(OH)_{12}(H_2O)_{12}$. *Can. Mineral.* **34**, 1071–1088.

Galuskin E., Armbruster T., Galuskina I., Lazic B., Winiarski A., Gazeev V. M., Dzierzanowski P., Zadov A. E., Pertsev N. N., Wrzalik R., Gurbanov A. G. and Janeczek J. (2011) Vorlanite $(CaU^{6+})O_4$ – A new mineral from the Upper Chegem caldera, Kabardino-Balkaria, Northern Caucasus, Russia. *Am. Mineral.* **96**, 188–196.

Gaona X., Dähn R., Tits J., Scheinost A. C. and Wieland E. (2011) Uptake of Np(IV) by C–S–H phases and cement paste: An EXAFS study. *Environ. Sci. Technol.* **45**, 8765–8771.

Geipel G., Reich T., Brendler V., Bernhard G. and Nitsche H. (1997) Laser and X-ray spectroscopic studies of uranium-calcite interface phenomena. *J. Nucl. Mater.* **248**, 408–411.

Giammar D. E. and Hering J. G. (2001) Time scales for sorption–desorption and surface precipitation of uranyl on goethite. *Environ. Sci. Technol.* **35**, 3332–3337.

Hay M. B., Workman R. K. and Manne S. (2003) Mechanisms of metal ion sorption on calcite: Composition mapping by lateral force microscopy. *Langmuir* **19**, 3727–3740.

Heberling F., Brendebach B. and Bosbach D. (2008) Neptunium(V) adsorption to calcite. *J. Contam. Hydrol.* **102**, 246–252.

Henrich B., Bergamaschi A., Broennimann C., Dinapoli R., Eikenberry E. F., Johnson I., Kobas M., Kraft P., Mozzanica A. and Schmitt B. (2009) PILATUS: A single photon counting pixel detector for X-ray applications. *Nucl. Instrum. Methods* **607**, 247–249.

Ilavsky J. and Jemian P. (2009) Irena: Tool suite for modeling and analysis of small-angle scattering. *J. Appl. Cryst.* **42**, 347–353.

Kelly S. D., Newville M. G., Cheng L., Kemner K. M., Sutton S. R., Fenter P., Sturchio N. C. and Spötl C. (2003) Uranyl incorporation in natural calcite. *Environ. Sci. Technol.* **37**, 1284–1287.

Macé N., Wieland E., Dähn R., Tits J. and Scheinost A. C. (2013) EXAFS investigation on U(VI) immobilization in hardened cement paste: Influence of experimental conditions on speciation. *Radiochim. Acta* **101**, 379.

Meece D. E. and Benninger L. K. (1993) The coprecipitation of Pu and other radionuclides with $CaCO_3$. *Geochim. Cosmochim. Acta* **57**, 1447–1458.

Missana T., Garcta-Gutiérrez M. and Maffiotte C. (2003) Experimental and modeling study of the uranium (VI) sorption on goethite. *J. Colloid Interface Sci.* **260**, 291–301.

Natrajan L. S. (2012) Developments in the photophysics and photochemistry of actinide ions and their coordination compounds. *Coordin. Chem. Rev.* **256**, 1583–1603.

NEA (2004) *Post-closure safety case for geological repositories: Nature and purpose*. OECD, Paris.

Novikov A. P., Kalmykov S. N., Utsunomiya S., Ewing R. C., Horreard F., Merkulov A., Clark S. B., Tkachev V. V. and Myasoedov B. F. (2006) Colloid transport of plutonium in the far-field of the mayak production association, Russia. *Science* **314**, 638–641.

Ong C. G. and Leckie J. O. (1996) Anion exchange preparation of a ^{232}U radiotracer for alpha-particle liquid scintillation counting. *Talanta* **43**, 601–605.

Parkman R. H., Charnock J. M., Livens F. R. and Vaughan D. J. (1998) A study of the interaction of strontium ions in aqueous solution with the surfaces of calcite and kaolinite. *Geochim. Cosmochim. Acta* **62**, 1481–1492.

Piret-Meunier J., Piret P. (1982) COD ID: 9012087. Crystallography Open Database.

Porcelli D., Andersson P. S., Wasserburg G. J., Ingri J. and Baskaran M. (1997) The importance of colloids and mires for the transport of uranium isotopes through the Kalix River watershed and Baltic Sea. *Geochim. Cosmochim. Acta* **61**, 4095–4113.

R-Core (2012) *R: A language and environment for statistical computing*. R Foundation for Statistical Computing, Vienna, Austria.

Ravel B. and Newville M. (2005) ATHENA, ARTEMIS, HEPHAESTUS: Data analysis for X-ray absorption spectroscopy using IFEFFIT. *J. Synchrotron Radiat.* **12**, 537–541.

Redmond M. P., Cornet S. M., Woodall S. D., Whittaker D., Collison D., Helliwell M. and Natrajan L. S. (2011) Probing the local coordination environment and nuclearity of uranyl(VI) complexes in non-aqueous media by emission spectroscopy. *Dalton Trans.* **40**, 3914–3926.

Reeder R., Nugent M., Lamble G., Tait C. D. and Morris D. (2000) Uranyl incorporation into calcite and aragonite: XAFS and luminescence studies. *Environ. Sci. Technol.* **34**, 638–644.

Reeder R., Nugent M., Tait C. D., Morris D., Heald S., Beck K., Hess W. and Lanzirotti A. (2001) Coprecipitation of Uranium(VI) with calcite: XAFS, micro-XAS, and luminescence characterization. *Geochim. Cosmochim. Acta* **65**, 3491–3503.

Reeder R., Elzinga E., Tait C. D., Rector K. D., Donohoe R. and Morris D. (2004) Site-specific incorporation of uranyl carbonate species at the calcite surface. *Geochim. Cosmochim. Acta* **68**, 4799–4808.

Reidy R. F., Allen A. J. and Krueger S. (2001) Small angle neutron scattering characterization of colloidal and fractal aerogels. *J. Non-Cryst. Solids.* **285**, 181–186.

Rihs S., Sturchio N., Orlandini K., Cheng L., Teng H., Fenter P. and Bedzyk M. (2004) Interaction of uranyl with calcite in the presence of EDTA. *Environ. Sci. Technol.* **38**, 5078–5086.

Rogova V. P., Belova L. N., Kiziyarov G. N. and Kuznetsova N. N. (1974) Bauranoite and metacalciouranoite, new minerals of the hydrous uranium oxides group. *Int. Geol. Rev.* **16**, 214–219.

Schindler M. and Putnis A. (2004) Crystal growth of schopiete on the (104) surface of calcite. *Can. Mineral.* **42**, 1667–1681.

Schmidt P. (1991) Small-angle scattering studies of disordered, porous and fractal systems. *J. Appl. Cryst.* **24**, 414–435.

Schwyn B., Wersin P., Rüedi J., Schneider J., Altmann S., Missana T. and Noseck U. (2012) FUNMIG Integrated Project results and conclusions from a safety case perspective. *Appl. Geochem.* **27**, 501–515.

Somasundaran P. and Agar G. E. (1967) The zero point of charge of calcite. *J. Colloid Interface Sci.* **24**, 433–440.

Tits J., Wieland E. and Bradbury M. H. (2005) The effect of isosaccharinic acid and gluconic acid on the retention of Eu(III), Am(III) and Th(IV) by calcite. *Appl. Geochem.* **20**, 2082–2096.

Tits J., Geipel G., Macé N., Elizer M. and Wieland E. (2011) Determination of uranium(VI) sorbed species in calcium silicate hydrate phases: A laser-induced luminescence spectroscopy and batch sorption study. *J. Colloid Interface Sci.* **359**, 248–256.

Wang Z., Zachara J. M., Liu C., Gassman P. L., Felmy A. R. and Clark S. B. (2008) A cryogenic fluorescence spectroscopic study of uranyl carbonate, phosphate and oxyhydroxide minerals. *Radiochim. Acta* **96**, 591–598.

Wieland E., Tits J. and Bradbury M. H. (2004) The potential effect of cementitious colloids on radionuclide mobilisation in a repository for radioactive waste. *Appl. Geochem.* **19**, 119–135.

Zachara J. M., Cowan C. E. and Resch C. T. (1991) Sorption of divalent metals on calcite. *Geochim. Cosmochim. Acta* **55**, 1549–1562.

Zachariasen W. H. (1948) Crystal chemical studies of the 5f-series of elements. IV. The crystal structure of $Ca(UO_2)O_2$ and $Sr(UO_2)O_2$. *Acta Cryst.* **1**, 281–285.

Zavarin M., Roberts S., Hakem N., Sawvel A. and Kersting A. (2005) Eu(III), Sm(III), Np(V), Pu(V), and Pu(IV) sorption to calcite. *Radiochim. Acta* **93**, 93–102.

Associate editor: Christopher Kim

U(VI) behaviour in hyperalkaline calcite systems

Kurt F. Smith[a,b], Nicholas D. Bryan[b,c], Adam N. Swinburne[c], Pieter Bots[a], Samuel Shaw[a], Louise S. Natrajan[c], J. Frederick W. Mosselmans[d], Francis R. Livens[a,c], and Katherine Morris*[a]

[a]Research Centre for Radwaste Disposal and Williamson Research Centre, School of Earth, Atmospheric and Environmental Sciences, The University of Manchester, Oxford Road, Manchester, M13 9PL, United Kingdom.

[b]National Nuclear Laboratory, Chadwick House, Risley, WA3 6AE, United Kingdom.

[c]Centre for Radiochemistry Research, School of Chemistry, The University of Manchester, Oxford Road, Manchester, M13 9PL, United Kingdom.

[d]Diamond Light Source Ltd., Diamond House, Harwell Science and Innovation Campus, Didcot, Oxfordshire, OX11 0DE. UK

*Corresponding author (katherine.morris@manchester.ac.uk)

Figure S1. Powder X-ray diffraction pattern collected from calcite used throughout this study

Figure S2. Energy dispersive X-ray spectrum collected from calcite sample and show peaks indicative of U.

Figure S3. Selected area electron diffraction data from uranium containing precipitate overlain with becquerelite crystallographic data.

Figure S4. Selected area electron diffraction data from uranium containing precipitate overlain with schoepite crystallographic data.

Figure S5. Selected area electron diffraction data from uranium containing precipitate overlain with $Ca_2U_2O_7$ crystallographic data.

Table S1. Kd values (kg L^{-1}) for U(VI)-calcite batch experiments

System	Solid : Solution	[U(VI)] (μM)			
		5.3×10^{-5}	**0.42**	**2.1**	**4.2**
OCL	**1:2**	12	-	-	-
	1:5	19	-	-	-
	1:10	15	9.4	33	68
	1:50	8.6	3.1	150	160
	1:500	2	1.8	200	33000
YCL	**1:2**	13	-	-	-
	1:5	18	-	-	-
	1:10	23	-	-	-
	1:50	8.6	-	-	-
	1:500	4.1	-	-	-

Table S2. Summary of luminescence and lifetime data

Sample	λ_{ex}(nm)	λ_{em} (nm)	$E_{0\text{-}0}$(cm^{-1})[a]	τ_1 (µs)[b]	τ_2 (µs)[b]	τ_3 (µs)[b]	k_1 (10^3 s^{-1})[c]
0.21 µM U(IV)	250	513	20 790	736 ± 12 (55%)	1290 ± 22 (45%)	-	0.77
0.42 µM U(IV)	250	513	20 330	141 ± 2 (32%)	515 ± 8 (68%)	-	1.94
2.10 µM U(IV)	250	538	20 330	26.0 ± 1.1 (6%)	94.5 ± 2.7 (35%)	422 ± 11 (57%)	2.37
4.20 µM U(IV)	250	525	20 750	22.1 ± 1.3 (13%)	105 ± 4 (52%)	319 ± 11 (36%)	3.13
OCL precipitate	250	535	20 920	23.0 ± 0.4 (47%)	75.2 ± 1.0 (53%)		13.3

Improved signal to noise was obtained using 250 nm excitation. [a]The apparent electronic origin values ($E_{0\text{-}0}$) were determined from the observed energy of the first vibronic band in the emission spectra. The exact location of $E_{0\text{-}0}$ is often difficult to ascertain in spectra of uranyl compounds especially at low resolution and its exact $E_{0\text{-}0}$ may lie at higher energies depending on the local symmetry of the species in question. [b]Lifetimes quoted are subject to the numerical error given after the lifetime and were collected at: 501 nm (0.21 µM sample); 500 nm (0.42 µM sample); 512 nm (2.10 µM sample); and 503 nm (4.20 µM sample). The relative percentage contributions of each exponential to the total intensity at time = 0 are given in brackets. [c]The radiative rate constant for the longest lived component in the kinetic trace reported.

Table S3. EXAFS best fit parameters for U(VI)-calcite samples with a single Oeq shell.

	42.0 µM (A)				21.0 µM (B)				Coprecipitated (C)			
	N	**R (Å)**		**σ^2 (Å^2)**	**N**	**R (Å)**		**σ^2 (Å^2)**	**N**	**R (Å)**		**σ^2 (Å^2)**
U-O_{ax}	2	1.8 ± 0.01		0.002 ± 0.001	2	1.81 ± 0.01		0.002 ± 0.001	2	1.81 ± 0.01		0.003 ± 0.001
U-O_{eq}	5	2.28 ± 0.02		0.011 ± 0.001	5	2.31 ± 0.02		0.010 ± 0.002	6	2.41 ± 0.02		0.011 ± 0.002
U-C									3	2.91 ± 0.03		0.008 ± 0.005
U-U_1	1	3.61 ± 0.07		0.008 ± 0.007	1	3.67 ± 0.06		0.006 ± 0.005				
U-U_2	3	3.82 ± 0.06		0.015 ± 0.001	3	3.88 ± 0.07		0.014 ± 0.009				
$S0^2$		0.92				0.9				0.9		
ΔE0		0.24				3.2				6.5		
Reduced χ^2		124				50.4				37.8		
R		0.03				0.04				0.02		

Coordination numbers for samples A and B were fixed to those found in becquerelite while sample C were fixed to those found in liebigite. A forward through absorber multiple scattering path was included for the axial oxygens in all systems.

Table S4. Saturation indices of various U(VI) solid phases in calcite equilibrated OCL systems.

U(VI) Phase	SI	
	4.20 μM	42.0 μM
Becquerelite (nat)	14.3	19.8
Becquerelite (syn)	2.80	8.30
$CaU_2O_7{:}3H_2O$ (cr)	2.59	4.43
UO_4Ca (cr)	5.73	6.66
Schoepite (des)	-	0.24
$UO_2(OH)_2$ (beta)	-	0.31

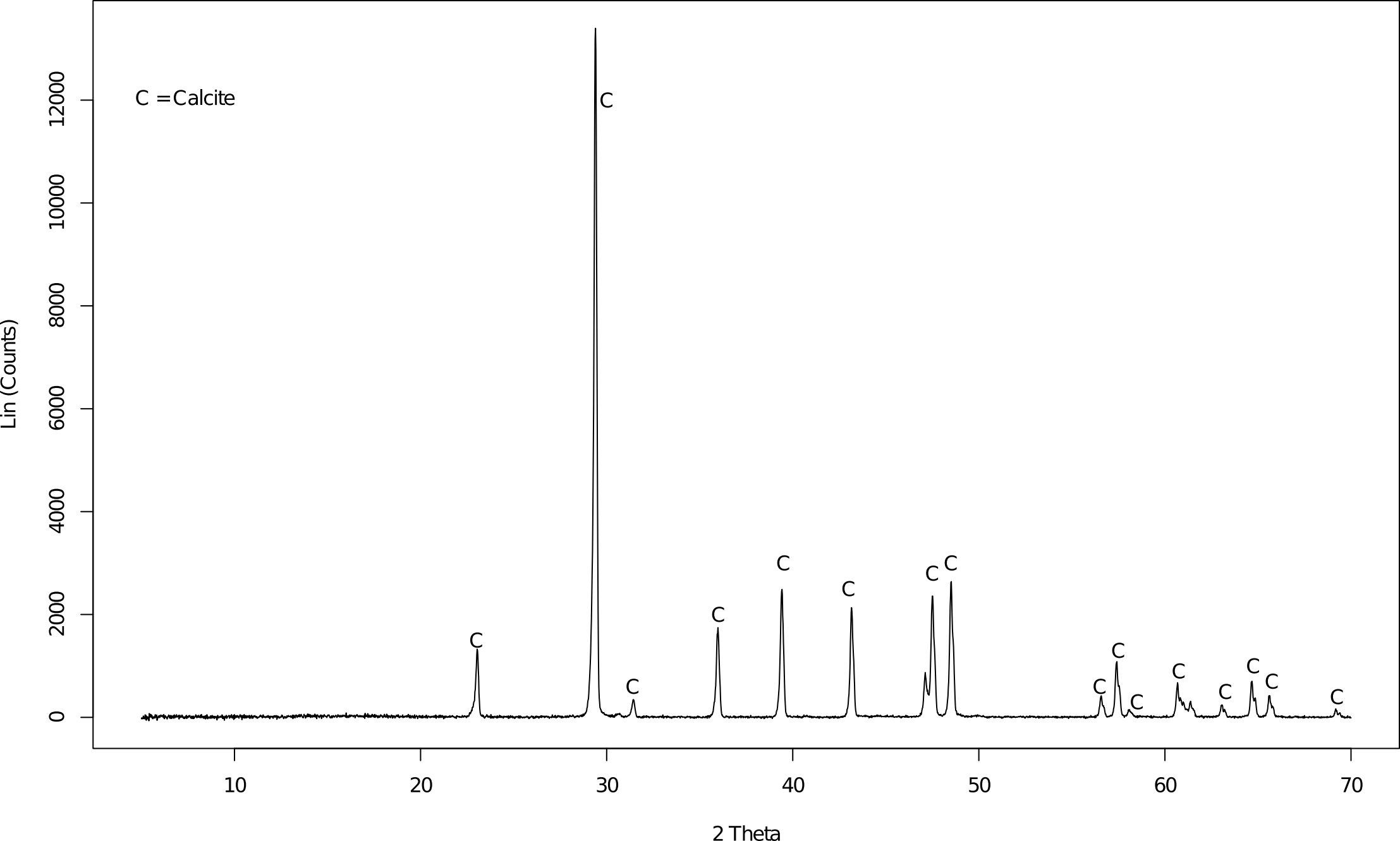
C =Calcite
C
C
C
C
C
C
C
C
C
C
C
C
C
C
C
C
C
C
C
0
2000
4000
6000
8000
10000
12000
Lin (Counts)
10
20
30
40
50
60
70
2 Theta

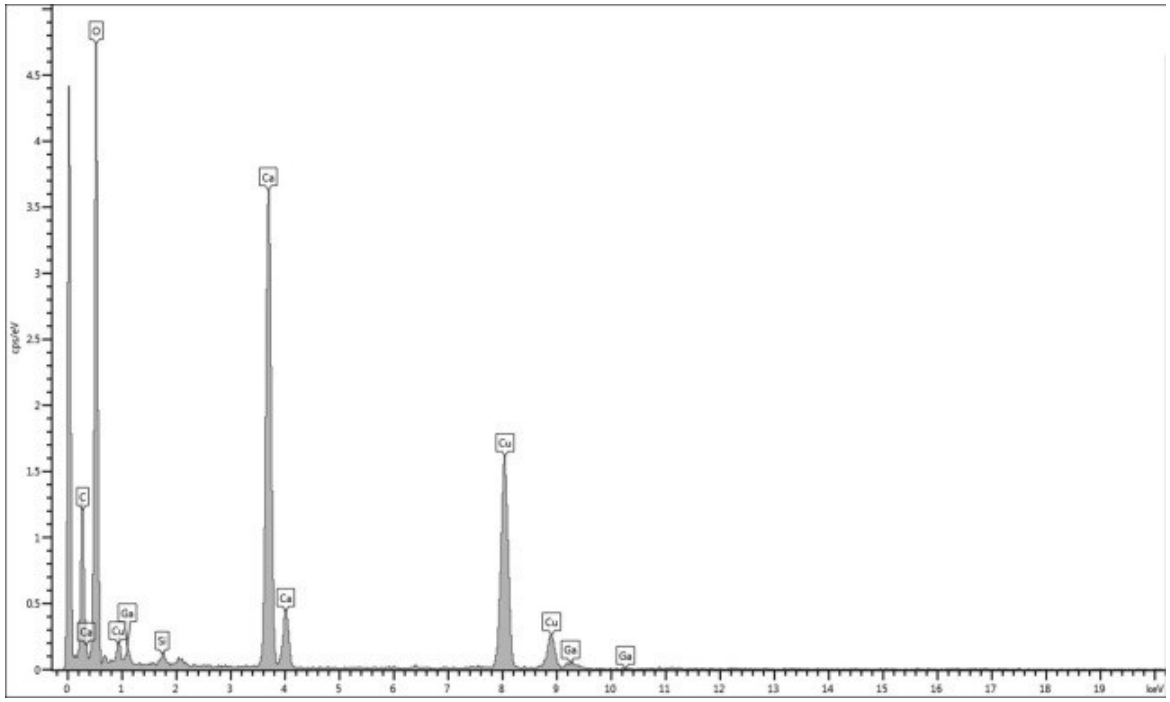

Supplementary Figure 2.

Kurt F. Smith, Nicholas D. Bryan, Adam N. Swinburne, Pieter Bots, Samuel Shaw, Louise S. Natrajan, J. Frederick W. Mosselmans, Francis R. Livens, Katherine Morris

U(VI) behaviour in hyperalkaline calcite systems

Geochimica et Cosmochimica Acta, Volume 148, 2015, 343–359

http://dx.doi.org/10.1016/j.gca.2014.09.043

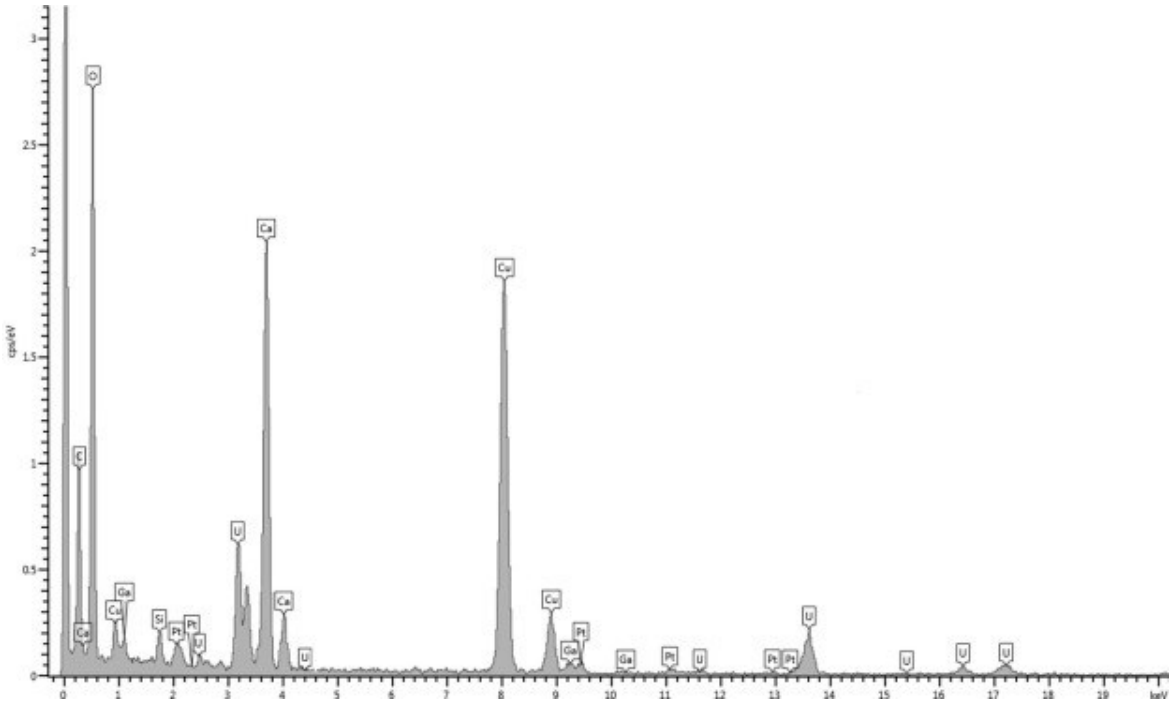

Supplementary Figure 3.

Kurt F. Smith, Nicholas D. Bryan, Adam N. Swinburne, Pieter Bots, Samuel Shaw, Louise S. Natrajan, J. Frederick W. Mosselmans, Francis R. Livens, Katherine Morris

U(VI) behaviour in hyperalkaline calcite systems

Geochimica et Cosmochimica Acta, Volume 148, 2015, 343–359

http://dx.doi.org/10.1016/j.gca.2014.09.043

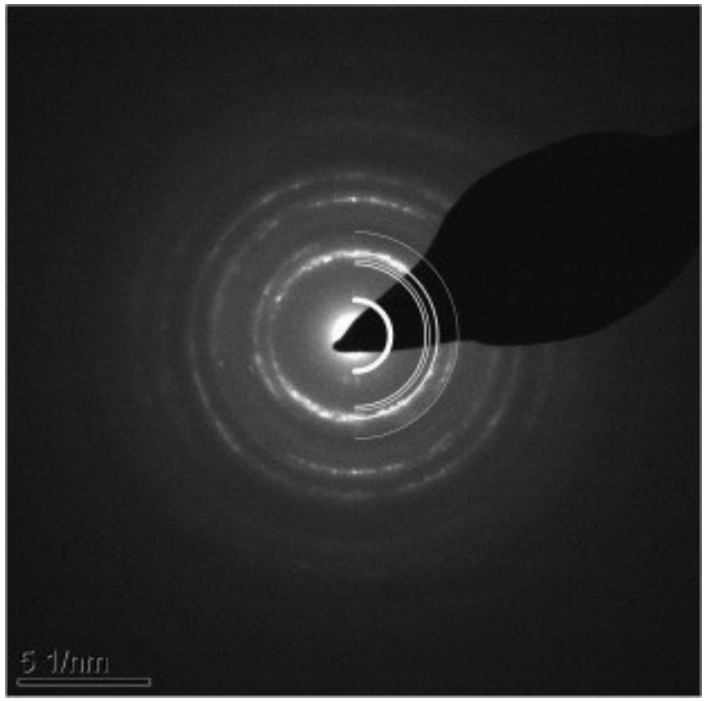

Supplementary Figure 4.

Kurt F. Smith, Nicholas D. Bryan, Adam N. Swinburne, Pieter Bots, Samuel Shaw, Louise S. Natrajan, J. Frederick W. Mosselmans, Francis R. Livens, Katherine Morris

U(VI) behaviour in hyperalkaline calcite systems

Geochimica et Cosmochimica Acta, Volume 148, 2015, 343–359

http://dx.doi.org/10.1016/j.gca.2014.09.043

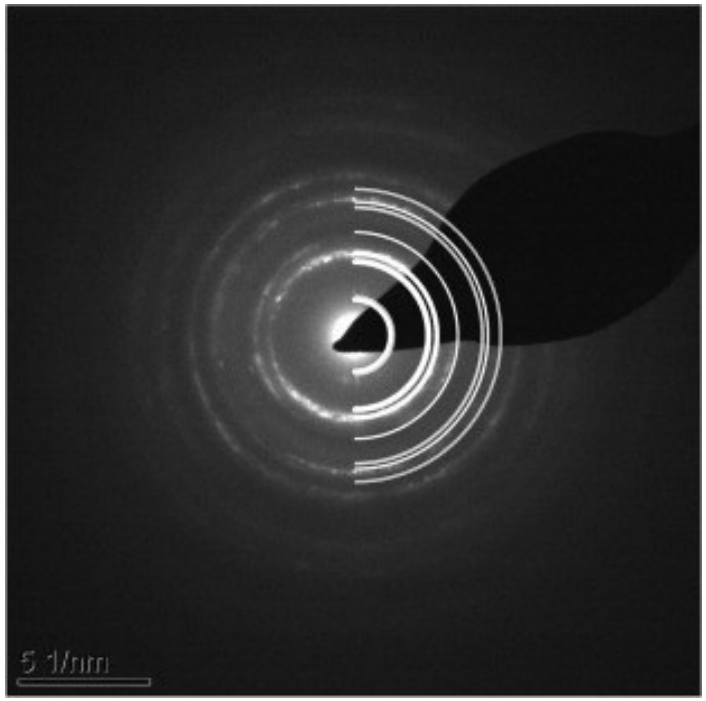

Supplementary Figure 5.

Kurt F. Smith, Nicholas D. Bryan, Adam N. Swinburne, Pieter Bots, Samuel Shaw, Louise S. Natrajan, J. Frederick W. Mosselmans, Francis R. Livens, Katherine Morris

U(VI) behaviour in hyperalkaline calcite systems

Geochimica et Cosmochimica Acta, Volume 148, 2015, 343–359

http://dx.doi.org/10.1016/j.gca.2014.09.043

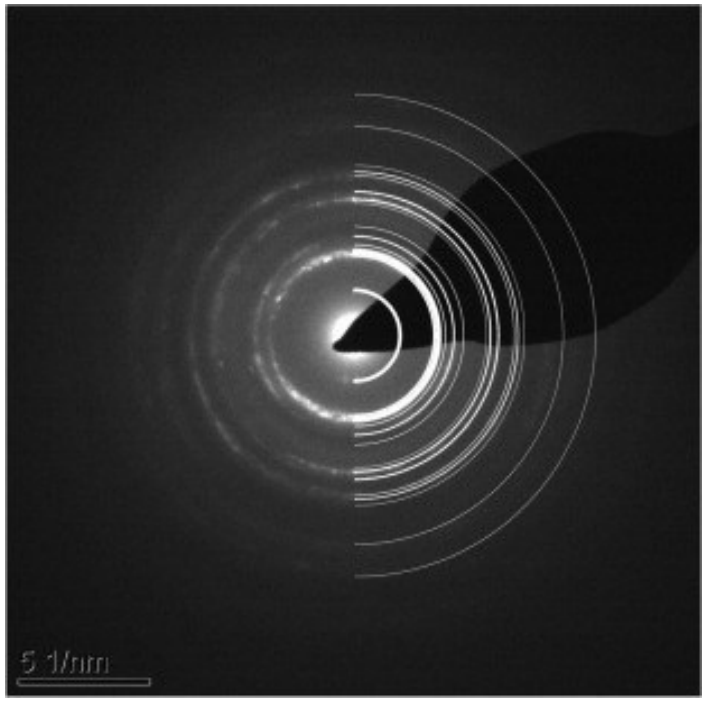

Supplementary Figure 6.

Kurt F. Smith, Nicholas D. Bryan, Adam N. Swinburne, Pieter Bots, Samuel Shaw, Louise S. Natrajan, J. Frederick W. Mosselmans, Francis R. Livens, Katherine Morris

U(VI) behaviour in hyperalkaline calcite systems

Geochimica et Cosmochimica Acta, Volume 148, 2015, 343–359

http://dx.doi.org/10.1016/j.gca.2014.09.043

Supplementary Figure 6.

Kurt F. Smith, Nicholas D. Bryan, Adam N. Swinburne, Pieter Bots, Samuel Shaw, Louise S. Natrajan, J. Frederick W. Mosselmans, Francis R. Livens, Katherine Morris

U(VI) behaviour in hyperalkaline calcite systems

Geochimica et Cosmochimica Acta, Volume 148, 2015, 343–359

http://dx.doi.org/10.1016/j.gca.2014.09.043